

# Stochastic Block Covariance Matrix Estimation

Yunran Chen<sup>1</sup>, Surya T Tokdar<sup>1,4</sup>, and Jennifer M Groh<sup>2,3,4,5</sup>

<sup>1</sup>Department of Statistical Science, Duke University, USA

<sup>2</sup>Department of Psychology & Neuroscience, Duke University, USA

<sup>3</sup>Department of Biomedical Engineering, Duke University, USA

<sup>4</sup>Duke Institute of Brain Sciences, Duke University, USA

<sup>5</sup>Center for Cognitive Neuroscience, Duke University, USA

February 18, 2025

## Abstract

Motivated by a neuroscience application we study the problem of statistical estimation of a high-dimensional covariance matrix with a block structure. The block model embeds a structural assumption: the population of items (neurons) can be divided into latent sub-populations with shared associative covariation within blocks and shared associative or dis-associative covariation across blocks. Unlike the block diagonal assumption, our block structure incorporates positive or negative pairwise correlation between blocks. In addition to offering reasonable modeling choices in neuroscience and economics, the block covariance matrix assumption is interesting purely from the perspective of statistical estimation theory: (a) it offers in-built dimension reduction and (b) it resembles a regularized factor model without the need of choosing the number of factors. We discuss a hierarchical Bayesian estimation method to simultaneously recover the latent blocks and estimate the overall covariance matrix. We show with numerical experiments that a hierarchical structure and a shrinkage prior are essential to accurate recovery when several blocks are present.

*Keywords:* covariance estimation, block structure regularization, Bayesian shrinkage prior

# 1 Introduction

It is well understood that an accurate estimation of a covariance matrix is infeasible without appropriate regularization when the number of variables  $p$  is comparable to or exceeds the sample size  $n$ . Regularization is typically enforced either through assumptions of sparsity, with known or unknown sparsity structures, or by the technique of shrinkage customized to specific composite loss functions and invariance constraints; see, for example, [Wu and Pourahmadi \(2003\)](#); [Ledoit and Wolf \(2004, 2020\)](#); [Zou et al. \(2006\)](#); [Bickel and Levina \(2008\)](#); [Rajaratnam et al. \(2008\)](#); [Cai et al. \(2010\)](#); [Bhattacharya and Dunson \(2011\)](#), and the references therein. [Cai et al. \(2016\)](#); [Fan et al. \(2016\)](#); [Pourahmadi \(2013\)](#) offer comprehensive reviews on the topic.

An approach that combines sparsity with shrinkage, but has received scant attention in the literature, is covariance estimation under stochastic block models. These models posit that the  $p$  variables are clustered into  $k$  distinct groups (blocks) such that the covariance (or correlation) between any pair of variables is entirely determined by their group memberships. Similar stochastic blockmodels are a popular choice for analyzing network data (see [Lee and Wilkinson, 2019](#), for a review), but it remains underappreciated that such models could bring about unexpected benefits in covariance estimation. [Liechty et al. \(2004\)](#) seem to be the first to use these models to group companies by stock price correlation and group plant phenotypes by size correlation. Crucially, in the second application, they identify two groups of phenotypes with negative cross-block correlation and conclude that plants either emphasize leaf growth or plant growth, but not both.

Relative to other blocking strategies ([Perrot-Dockes et al., 2022](#)), the stochastic block covariance model is unique in its twofold ability to identify suitable clusters and detect cross-block negative correlation – two features of immense importance to many areas of science. Our study of these models is motivated by neuroscience research where we investigate how a population of neurons coordinate with one another to preserve information from multiple stimuli presented simultaneously. [Jun et al. \(2022\)](#) observe a bimodal distribution of pairwise spike count correlations under dual-stimuli exposures and suggest the existence of subpopulations with synchronous encoding within groups and anti-synchronous activities across – a conjecture which can be more comprehensively tested with the stochastic block covariance model. Correlation clustering could also be useful beyond hypothesis testing. In finance, for example, accurate clustering of assets could facilitate portfolio diversification and risk mitigation ([Creal and Kim, 2024](#)).

Beyond its scientific appeal, stochastic block covariance estimation is interesting purely as a statistical tool because of its ability to synthesize shrinkage with sparsity. Sparsity is explicitly encoded by the structural assumption of  $k$  blocks. One only needs to estimate  $k(k + 3)/2$  distinct parameters –  $k$  block level variances and  $k(k + 1)/2$  within and cross-block covariances – instead of  $p(p + 1)/2$  free parameters in a  $p \times p$  covariance matrix. The role of shrinkage is more implicit. [Theorem 2.1](#) shows that given the grouping structure, the maximum likelihood estimate of the covariance matrix is obtained by simply averaging the raw sample variances and covariances within and across the groups. This averaging is a shrinkage operation and for it to work one must shrink adaptively by identifying a good partition of the variables so that within and across block averaging does not degrade fidelity between data and the estimate. How to shrink adaptively is the main question we address in this paper ([Section 3](#)). Stochastic block covariance models also have close connection with regularized factor models ([Taylor-Rodríguez et al., 2017](#); [Tong and Hansen, 2023](#)) but, arguably, offer a more efficient estimation framework as examined in [Section 5.1](#).

Clearly, the primary challenge with stochastic block covariance matrix estimation is identifi-

cation of the blocks which itself constitutes of two interrelated questions. How many blocks are needed? How to assign variables to blocks? It is appealing to address these challenges with a Bayesian approach where one can specify a prior distribution on the space of partitions of the variable indices. But a Bayesian approach presents a new technical challenge. One also needs a prior distribution on the space of block covariance matrices which is a highly constrained subspace of the space of  $p \times p$  positive semidefinite matrices. [Liechty et al. \(2004\)](#) use truncation to circumvent the technical issue of constraints but the resulting posterior computation is both complex and limited in scope. Indeed, [Liechty et al. \(2004\)](#) do not fully address the question of *how many blocks are needed*; they assume a number is known from the context of the application.

A more fruitful solution is offered by [Creal and Kim \(2024\)](#) who exploit a novel matrix factorization result of [Archakov and Hansen \(2024\)](#) to specify a conjugate prior on the block covariance matrix given a known partition of the variables. This specification enables to calculate – in closed form – the marginal likelihood score of a given partition. The marginal likelihood is then combined with a partition prior to make inference on the blocks with straightforward Markov chain Monte Carlo computation (e.g. [Miller and Harrison, 2018](#)). The posterior mean – which averages over likely partitions – is the Bayes estimate of the covariance matrix under squared Frobenius loss.

While such Bayes estimates are a type of shrinkage estimates, they may fail to offer adaptive shrinkage in the learning of the blocks. Conditionally on a given partition, the mean of the conjugate prior provides a focal point of shrinkage of the pairwise covariance values and the prior variance controls the degree of shrinkage. For example one could specify a hyper-inverse Wishart  $g$ -prior ([Carvalho and Scott, 2009](#)) to shrink towards the conditional maximum likelihood estimate but such a specification would bias the method toward identifying a large number of blocks, resulting in poor quality of covariance estimation (Section 6.1). At the other end, [Creal and Kim \(2024\)](#) choose a prior specification which conditionally shrinks cross-block covariance values to zero, biasing the method toward detecting a small number of large blocks and again resulting in suboptimal performance when the true covariance matrix is better expressed as having many blocks with some negative cross-block covariances. Having adaptive shrinkage requires a prior specification which chooses both the shrinkage target and shrinkage intensity based on the data in a way that the resulting covariance estimate retains accuracy across a variety of true scenarios.

We introduce such an adaptive method for stochastic block covariance estimation within an empirical Bayesian framework by utilizing a hierarchical prior which promotes an additional layer of shrinkage: conditionally on the partition, the block covariance matrix estimate is biased toward the subspace of homogeneous block matrices. A formal definition is given in Section 3, with the implication that a homogeneous block covariance matrix has the same within and across covariance values. We perform a detailed numerical experiment to show that the ability to shrink toward a sparse subspace – rather than a single element with block diagonal structure – and the ability to determine how much to shrink are crucial to offering excellent adaptive performance in estimating block covariance matrices with many blocks and possibly negative cross-block correlations (Section 4.1). More interestingly, even when the true covariance matrix is not of block structure, the estimation accuracy of our method is comparable to or better than most existing methods, except in a few cases where strong prior information is available on a specific structure of sparsity (Section 4.2.3). In Section 6.1 we apply the new method to the motivating neuroscience study and identify neuron subpopulations with both positive and negative cross-correlations, some of which are missed by the method of ([Creal and Kim, 2024](#)). In Section 6.2, we revisit the industry classification example studied by [Liechty et al. \(2004\)](#), but in a more flexible way that does not prefix the

number of clusters. In Section 6.3, we employ the proposed method to explore differences in phenotypic integration in plants under contrasting environmental conditions, providing an alternative perspective to the analysis carried out by Matesanz et al. (2021). We conclude in Section 7 with some remarks on remaining challenges and potential future research directions.

## 2 Stochastic Block Covariance Estimation

We start with the fundamentals of stochastic block covariance model and Bayesian estimation strategies. Much of the discussion in this section is overlapping with Creal and Kim (2024) but we add some novel statistical insights such as Theorem 2.1. The concepts and notations from this section are going to be useful for our original research on shrinkage presented in the next few sections.

### 2.1 Preliminaries of block covariance structure

We call a  $p \times p$  positive semidefinite matrix  $\Gamma$  a block covariance matrix if there exist positive integers  $k$  and  $p_1, \dots, p_k$  with  $p_1 + \dots + p_k = p$ , such that  $\Gamma$  can be partitioned as

$$\Gamma = \begin{pmatrix} \Gamma_{[1,1]} & \Gamma_{[1,2]} & \dots & \Gamma_{[1,k]} \\ \Gamma_{[2,1]} & \Gamma_{[2,2]} & \dots & \Gamma_{[2,k]} \\ \vdots & \vdots & \ddots & \vdots \\ \Gamma_{[k,1]} & \Gamma_{[k,2]} & \dots & \Gamma_{[k,k]} \end{pmatrix}, \quad \begin{aligned} \Gamma_{[u,u]} &= (\gamma_u^2 - \gamma_{uu})I_{p_u} + \gamma_{uu}J_{p_u \times p_u}, \\ \Gamma_{[u,v]} &= \gamma_{uv}J_{p_u \times p_v}, \quad u \neq v, \end{aligned} \quad (1)$$

where  $I_m$  denotes the  $m \times m$  identity matrix,  $J_{r \times s}$  denote the  $r \times s$  matrix of ones,  $\gamma_u^2$  is the common variance of variables in block  $u$ ,  $\gamma_{uu}$  is the common within block covariance in block  $u$ , and  $\gamma_{uv}$  is the shared pairwise cross-covariance between blocks  $u$  and  $v$ . Here,  $p_u$  denotes the size of group  $u$  and  $k$  represents the number of blocks. Let  $\mathbb{B}$  denote the space of all  $p \times p$  block covariance matrices.

Throughout we assume that data consists of  $n$  independent copies  $\mathbf{y}_1, \dots, \mathbf{y}_n$  of a random vector  $\mathbf{y} \in \mathbb{R}^p$  with  $E(\mathbf{y}) = 0$  and  $\text{Var}(\mathbf{y}) = \Sigma$  for some positive definite matrix  $\Sigma$ . We will estimate  $\Sigma$  under the Gaussian sampling model

$$\mathbf{y} \sim N(0, \Sigma), \quad P\Sigma \in \mathbb{B}, \quad \text{for some rotation matrix } P. \quad (2)$$

Any matrix  $\Sigma$  satisfying (2) will be called a *group covariance matrix*, i.e., a covariance matrix which could be rotated into a block covariance matrix. Notice that the rotation matrix is not uniquely determined. However, if  $\Sigma$  is a group covariance matrix, then there exists a unique and irreducible partition  $\mathcal{B} = \{B_1, \dots, B_k\}$  of the indices  $\{1, \dots, p\}$  for some positive integer  $k$  such that  $\Gamma = \text{Var}(P_{\mathcal{B}}\mathbf{y})$  is a block covariance matrix with  $k$  blocks of sizes  $p_u = |B_u|$ , where  $P_{\mathcal{B}}$  is the rotation matrix determined by any permutation  $\sigma_{\mathcal{B}}$  of  $\{1, \dots, p\}$  such that  $\sigma_{\mathcal{B}}(B_u) = \{\sum_{v < u} p_v + j : 1 \leq j \leq p_u\}$ ,  $1 \leq u \leq k$ . Neither  $P_{\mathcal{B}}$  nor  $\Gamma$  is uniquely determined by a group covariance matrix  $\Sigma$  but the partition  $\mathcal{B}$  is. Indeed,  $\mathcal{B}$  can be recovered from  $\Sigma = ((\sigma_{ij}))$  by partitioning  $\{1, \dots, p\}$  according to the equivalence relation:  $i \sim j$  if and only if  $\sigma_{ii} = \sigma_{jj}$ ,  $\sigma_{il} = \sigma_{jl}$  for every  $l \notin \{i, j\}$ . This issue of identifiability will be important in our subsequent treatment.

## 2.2 Semi-spectral decomposition of a block covariance matrix

For a  $\Gamma \in \mathbb{B}$  to be positive semidefinite there have to be restrictions on what values  $\gamma_u^2, \gamma_{uu}, \gamma_{uv}$  can take. These restrictions can be considerably simplified by using the following semi-spectral factorization ([Archakov and Hansen, 2024](#))

$$\Gamma = QDQ', \quad (3)$$

where  $D$  is a pseudo-diagonal matrix and  $Q$  is a  $p \times p$  block-sparse orthonormal matrix ( $Q'Q = QQ' = I_p$ ) given as follows:

$$D = \begin{pmatrix} A & & & & & \\ & \lambda_1 I_{p_1-1} & & & & \\ & & \ddots & & & \\ & & & & \lambda_k I_{p_k-1} & \\ & & & & & \end{pmatrix} Q = \begin{pmatrix} Q_1^{(p_1)} & & & & & \\ & Q_1^{(p_2)} & & & & \\ & & \ddots & & & \\ & & & & Q_{-1}^{(p_1)} & \\ & & & & & Q_{-1}^{(p_2)} \\ & & & & & \ddots \\ & & & & & & Q_{-1}^{(p_k)} \end{pmatrix},$$

with  $A = ((a_{uv}))_{k \times k}$  and  $\lambda_1, \dots, \lambda_k$  defined by

$$\lambda_u = \gamma_u^2 - \gamma_{uu}, \quad a_{uu} = \gamma_u^2 + (p_u - 1)\gamma_{uu}, \quad a_{uv} = \gamma_{uv}\sqrt{p_u p_v}, \quad u \neq v, \quad (4)$$

and  $Q_1^{(p_u)} = J_{p_u \times 1} / \sqrt{p_u}$  and  $Q_{-1}^{(p_u)}$  chosen such that the matrix  $Q^{(p_u)} = [Q_1^{(p_u)} \quad : \quad Q_{-1}^{(p_u)}]$  are orthonormal matrices.

It is easy to see that  $\Gamma$  is positive semidefinite if and only if  $A$  is positive semidefinite and  $\lambda_1, \dots, \lambda_k$  are nonnegative. Indeed, if  $\mathbf{z} = (z_1, \dots, z_p)'$  is a random vector with  $\text{Var}(\mathbf{z}) = \Gamma$  then  $\text{Var}(Q'\mathbf{z}) = D$ . While such a result is reminiscent of the standard spectral decomposition of an arbitrary covariance matrix, a clear advantage of the block assumption is that the orthonormal matrix  $Q$  is fully determined by the block sizes alone. Given the blocks, estimation can focus on the  $k(k+3)/2$  many non-zero elements of the matrix  $D$  which also has a simple interpretation as the variance matrix of the rotated vector  $Q'\mathbf{z}$ . For example, the non-zero elements of  $D$  could be estimated by the corresponding sample quantities of  $Q'\mathbf{z}$ . The next Subsection explores this in more detail. It is worth noting here that  $Q$  is not unique except the first  $k$  columns which are unique up to sign change. Given block sizes  $p_1, \dots, p_k$ , one possible version of  $Q$  could be constructed using the Gram-Schmidt method; see Examples provided in equations (25) and (26) in the appendix.

## 2.3 Estimation of group covariance matrix with known groups

When the partition  $\mathcal{B} = \{B_1, \dots, B_k\}$  is known, the observation vector  $\mathbf{y}$  can be rotated to  $\mathbf{z} = P_{\mathcal{B}}\mathbf{y}$  and the observation model could be rewritten as  $\mathbf{z} \sim N(0, \Gamma)$ ,  $\Gamma \in \mathbb{B}$ , with  $p_u = |B_u|$ ,  $1 \leq u \leq k$ . The semi-spectral decomposition result then gives  $\Gamma = QDQ'$  with  $Q$  being a known orthogonal matrix and  $D$  an unknown block diagonal matrix determined by a  $k \times k$  positive semidefinite matrix  $A$  and  $k$  nonnegative numbers  $\lambda_1, \dots, \lambda_k$ . The laws of large numbers imply that  $\hat{D}$ , which estimates the non-zero elements of  $D$  by the corresponding sample quantities of  $Q'\mathbf{z}$ , gives a consistent estimate of  $D$  as sample size  $n \rightarrow \infty$  for a fixed dimension  $p$ . The estimate  $\hat{D}$  is also the maximum likelihood estimate of  $D$  under the Gaussian model.

Given the known partition  $\mathcal{B} = (B_1, \dots, B_k)$  take  $\mathbf{z}_i = P_{\mathcal{B}}\mathbf{y}_i$ ,  $i = 1, \dots, n$ . Find  $Q$  in the semi-spectral decomposition, which only depends on the total number of blocks  $k$  and the block sizes  $p_1, \dots, p_k$ . Define  $\boldsymbol{\eta}_i = Q'\mathbf{z}_i$ . Partition each rotated vector  $\boldsymbol{\eta}_i$  as  $\boldsymbol{\eta}'_i = (\boldsymbol{\eta}'_{i(0)}, \boldsymbol{\eta}'_{i(1)}, \dots, \boldsymbol{\eta}'_{i(k)})$  where  $\boldsymbol{\eta}'_{i(0)}$  is of length  $k$  and  $\boldsymbol{\eta}'_{i(u)}$  is of length  $p_u - 1$ ,  $u = 1, \dots, k$ . The log-likelihood function can be written as

$$\text{loglik} \doteq -\frac{n}{2} \log |A| - \frac{1}{2} \sum_{i=1}^n \boldsymbol{\eta}'_{i(0)} A^{-1} \boldsymbol{\eta}_{i(0)} - \frac{n}{2} \sum_{u=1}^k (p_u - 1) \log \lambda_u - \frac{1}{2} \sum_{i=1}^n \sum_{u=0}^k \frac{\|\boldsymbol{\eta}_{i(u)}\|^2}{\lambda_u}, \quad (5)$$

where  $\doteq$  denotes equality up to an additive constant. By taking the derivatives of the log-likelihood with respect to  $A$  and the  $\lambda_k$ 's respectively, we can obtain the maximum likelihood estimator

$$\hat{A} = \frac{\sum_{i=1}^n \boldsymbol{\eta}_{i(0)} \boldsymbol{\eta}'_{i(0)}}{n}, \quad \hat{\lambda}_u = \frac{\sum_{i=1}^n \|\boldsymbol{\eta}_{i(u)}\|^2}{n(p_u - 1)} \quad (6)$$

which are precisely the non-zero elements of  $\hat{D}$ .

The above result about  $\hat{D}$  is presented in Archakov and Hansen (2024) (see Theorem 3), but they do not explore properties of the corresponding estimate  $\hat{\Gamma} = Q'\hat{D}Q$  of  $\Gamma$  or that of  $\hat{\Sigma} = P'_{\mathcal{B}}\hat{\Gamma}P_{\mathcal{B}}$ . The theorem below, which seems to be new to the literature, shows that  $\hat{\Sigma}$  could be computed simply by replacing the blocks of the sample covariance matrix  $S = \sum_i \mathbf{y}_i \mathbf{y}'_i / n$  with block level averages.

**Theorem 2.1.**  $\hat{\Gamma} = Q\hat{D}Q'$  has the same block structure (1) as of  $\Gamma$  with  $\gamma_w^2$ ,  $\gamma_{uu}$ ,  $\gamma_{uv}$  replaced with the following estimates

$$\hat{\gamma}_u^2 = \frac{\sum_{j \in B_u} S_{jj}}{p_u}, \quad \hat{\gamma}_{uu} = \frac{\sum_{j \neq j' \in B_u} S_{jj'}}{p_u(p_u - 1)}, \quad \hat{\gamma}_{uv} = \frac{\sum_{j \in B_u, j' \in B_v} S_{jj'}}{p_u p_v} \text{ if } u \neq v.$$

Accordingly, the elements of  $\hat{\Sigma} = ((\hat{\sigma}_{ij}))$  are

$$\hat{\sigma}_{ij} = \begin{cases} \frac{\sum_{l \in B_u} S_{ll}}{p_u} & \text{if } i = j \in B_u \\ \frac{\sum_{l \neq l' \in B_u} S_{ll'}}{p_u(p_u - 1)} & \text{if } i \neq j \in B_u, \\ \frac{\sum_{l \in B_u, l' \in B_v} S_{ll'}}{p_u p_v} & \text{if } i \in B_u, j \in B_v, u \neq v. \end{cases}$$

A proof is presented in Appendix B. Notice again that  $\hat{\Sigma}$  is free of ambiguity regarding  $P_{\mathcal{B}}$  or  $\Gamma$ . At this point it might be tempting to think that the maximum likelihood framework could be extended also learn about the blocks  $\mathcal{B}$  by considering the profile loglikelihood  $L^*(\mathcal{B}) = \max_{\Sigma} p(Y|\Sigma, \mathcal{B}) \propto |\hat{A}|^{-n/2} \prod_{u=1}^k \hat{\lambda}_u^{-n(p_u-1)2}$ . However, estimation of  $\mathcal{B}$  based on  $L^*(\mathcal{B})$  suffers massively from the curse of dimensionality – the profile likelihood favors putting each variable in its own cluster with  $k \approx p$  and  $\hat{\Sigma} \approx S$ , and fails to offer any useful regularization (not reported here). A much more useful framework could be constructed by turning to a Bayesian formulation which offers natural protections against the curse of dimensionality by replacing the profile likelihood with a marginal likelihood obtained by integrating over  $p(Y|\Sigma, \mathcal{B})$  with respect to a prior  $p(\Sigma|\mathcal{B})$  (Jefferys and Berger, 1992). It turns out that for the current problem, a rich class of conjugate prior distributions are available for  $p(\Sigma|\mathcal{B})$ , which not only leads to an easy estimation of  $\Sigma$

given  $\mathcal{B}$ , but also an easy calculation of the marginal likelihood  $p(Y|\mathcal{B}) = \int p(Y|\Sigma, \mathcal{B})p(\Sigma|\mathcal{B})d\Sigma$ . This is what we discuss next.

## 2.4 Conjugate prior under known groups

A quick inspection of the log-likelihood formula (5) reveals that when the grouping structure  $\mathcal{B} = \{B_1, \dots, B_k\}$  is known with  $p_u = |B_u|$ ,  $1 \leq u \leq k$ , the specification

$$(A, \lambda_1, \dots, \lambda_k) | \mathcal{B} \sim IW(\nu_0 + k + 1, \nu_0 A_0) \times \otimes_{u=1}^k IG\left(\frac{s_{0,u}+2}{2}, \frac{s_{0,u}\lambda_{0,u}}{2}\right), \quad (7)$$

gives a conjugate prior distribution for  $A$  and  $\lambda_1, \dots, \lambda_u$ , with the posterior distribution given  $Y = (\mathbf{y}_1, \dots, \mathbf{y}_n)$  equaling

$$(A, \lambda_1, \dots, \lambda_k) | (Y, \mathcal{B}) \sim IW(\nu_n + k + 1, \nu_n A_n) \times \otimes_{u=1}^k IG\left(\frac{s_{n,u}+2}{2}, \frac{s_{n,u}\lambda_{n,u}}{2}\right), \quad (8)$$

with the usual updates

$$\begin{aligned} \nu_n &= \nu_0 + n, & \nu_n A_n &= \nu_0 A_0 + n \hat{A}, \\ s_{n,u} &= s_{0,u} + n(p_u - 1), & s_{n,u} \lambda_{n,u} &= s_{0,u} \lambda_{0,u} + n(p_u - 1) \hat{\lambda}_u \end{aligned}$$

where  $\hat{A}$  and  $\hat{\lambda}_u$  are as before.

As an estimate of  $\Sigma$  one could take the posterior mean  $\Sigma_n = E(\Sigma|Y, \mathcal{B}) = P'_B \Gamma_n P_B$  with  $\Gamma_n = Q D_n Q'$  where  $D_n$  is block diagonal with blocks  $(A_n, \lambda_{n,1} I_{p_1-1}, \dots, \lambda_{n,K} I_{p_K-1})$ . Clearly,

$$\Sigma_n = \alpha_n \Sigma_0 + (1 - \alpha_n) \hat{\Sigma}$$

where  $\alpha_n = \nu_0 / (\nu_0 + n) \in (0, 1)$ ,  $\hat{\Sigma}$  is as before, and  $\Sigma_0 = P'_B \Gamma_0 P_B$  with  $\Gamma_0 = Q D_0 Q'$  where  $D_0$  is the block diagonal matrix with blocks  $(A_0, \lambda_{0,1} I_{p_1-1}, \dots, \lambda_{0,k} I_{p_k-1})$ . An interesting choice of the hyperparameters is the data dependent choice:  $\nu_0 = g^{-1}n$ ,  $s_{0,u} = g^{-1}n(p_u - 1)$ ,  $A_0 = \hat{A}$ ,  $\lambda_{0,u} = \hat{\lambda}_u$ , which gives  $\Sigma_n = \Sigma_0 = \hat{\Sigma}$ . We will refer to this as the hyper-inverse Wishart  $g$ -prior following by [Carvalho and Scott \(2009\)](#) who used similar constructions for graph learning.

Conjugacy is salient in the present context on two accounts. It shows that a prior distribution can be constructed easily and directly on the space of a group covariance matrices with known grouping structure, and thus, offering significant improvement over the ad hoc and truncation-based construction of [Liechty et al. \(2004\)](#). Second, and this point is crucial, a marginal likelihood for the block partition  $\mathcal{B} = \{B_1, \dots, B_k\}$  can be calculated by integrating out  $A$  and  $\lambda_1, \dots, \lambda_k$ :

$$p(Y|\mathcal{B}) = (2\pi)^{-\frac{np}{2}} \times 2^{\frac{nk}{2}} \times \frac{|\nu_0 A_0|^{\frac{\nu_0}{2}} \Gamma_k\left(\frac{\nu_0}{2}\right)}{|\nu_n A_n|^{\frac{\nu_n}{2}} \Gamma_k\left(\frac{\nu_n}{2}\right)} \prod_{u=1}^k \frac{\Gamma\left(\frac{s_{n,u}}{2}\right) \left(\frac{s_{0,u}\lambda_{0,u}}{2}\right)^{\frac{s_{0,u}}{2}}}{\Gamma\left(\frac{s_{0,u}}{2}\right) \left(\frac{s_{n,u}\lambda_{n,u}}{2}\right)^{\frac{s_{n,u}}{2}}} \quad (9)$$

Note that the marginal likelihood  $p(Y|\mathcal{B})$  is free of any issues of identifiability, because  $\mathcal{B}$  is uniquely determined by a group covariance matrix  $\Sigma$ . We discuss next how this likelihood function could be combined with an appropriate prior on  $\mathcal{B}$  to carry out posterior inference on the blocks.

## 2.5 Estimation of blocks under partition priors

For our purposes it would be desirable for a prior distribution on  $\mathcal{B}$  to be invariant under permutation of the variable indices  $1, \dots, p$ . Probability distributions satisfying this permutation invariance property are referred to as exchangeable partition probability functions (EPPF) as introduced by [Kingman \(1978\)](#) and refined thereafter by many other authors; see [Pitman \(2006\)](#) for a review. EPPFs have a close connection to complete random measures which are routinely used in Bayesian mixture models, with the Dirichlet process mixtures ([Ferguson, 1973](#); [Antoniak, 1974](#)) and its generalizations ([Pitman and Yor, 1997](#)) being the most widely known examples. In this article we work with the *mixture of finite mixtures* (MFM) partition distribution ([Miller and Harrison, 2018](#)) which, compared to Dirichlet process mixtures, offers a greater control on the number of blocks and favors partitions with blocks of similar sizes. Its EPPF is given as

$$p(\mathcal{B}) = p(B_1, \dots, B_k) = V_p(k) \prod_{u=1}^k \rho^{(|B_u|)} \quad (10)$$

with  $V_p(k) = \sum_{u=1}^{\infty} f(u)u_{(k)}/(\rho u)^{(p)}$  where  $x^{(k)} := x(x+1)\cdots(x+k-1)$  and  $x_{(k)} = x(x-1)\cdots(x-k+1)$ , and  $f(k)$  is any strictly positive probability mass function on  $\{1, 2, \dots\}$  such that  $\sum_{k=1}^{\infty} f(k)$  converge to 1 reasonably quickly. The parameter  $\rho$  is a type of concentration parameter. Larger values of  $\rho$  favor blocks of more equal size.

By combining such a prior on  $\mathcal{B}$  with the conjugate prior in (7) and the marginal likelihood  $p(Y|\mathcal{B})$  from earlier, one obtains the posterior distribution of  $\mathcal{B}$  as  $p(\mathcal{B}|Y) \propto p(\mathcal{B})p(Y|\mathcal{B})$ , which could be used to estimate  $\Sigma$  as  $\bar{\Sigma} := E(\Sigma|Y) = \sum_{\mathcal{B}} E(\Sigma|Y, \mathcal{B})p(\mathcal{B}|Y)$ , with  $E(\Sigma|Y, \mathcal{B})$  as described before. As is typical in Bayesian estimation,  $\bar{\Sigma}$  could be approximated by Markov chain Monte Carlo (MCMC) as  $\bar{\Sigma} \approx (1/T) \sum_{t=1}^T E(\Sigma|\mathcal{B} = \mathcal{B}^{(t)})$ , where  $(\mathcal{B}^{(t)}, t = 1, 2, \dots)$  is an ergodic Markov chain with  $p(\mathcal{B}|Y)$  as its stationary distribution.

For the MFM prior, such a Markov chain can be easily constructed and sampled from by using Gibbs sampling. Indeed, if we choose  $f(k)$  to be the unit mean Poisson distribution shifted to the right by 1, then a random element  $\mathcal{B}$  drawn from the MFM EPPF can be described as follows

$$\begin{aligned} k^* &\sim f \\ (\pi_1, \dots, \pi_{k^*}) &\sim \text{Dir}_{k^*}(\rho, \dots, \rho) \\ c_1, \dots, c_p &\sim \text{Mult}(\pi) \\ \mathcal{B} &= \text{partition}(i \sim j \text{ iff } c_i = c_j) \end{aligned} \quad (11)$$

where the partition operation in the last step simply divides the indices  $1, \dots, p$  into disjoint non-empty subsets according to ties in the corresponding labels  $c_1, \dots, c_p$  generated in the previous step. Note that  $\mathcal{B} = \{B_1, \dots, B_k\}$  for some  $1 \leq k \leq k^*$ . A Gibbs chain with  $p(\mathcal{B}|Y)$  as its stationary distribution can be constructed as follows; see [Miller and Harrison \(2018\)](#) for technical details.

1. Initialize  $\mathcal{B}^{(0)} = \{\mathcal{B}_1^{(0)}, \dots, \mathcal{B}_k^{(0)}\}$  as an arbitrary partition of  $\{1, \dots, p\}$  and create labels  $c_1, \dots, c_p$  so that  $c_i = c_j$  if and only if  $i$  and  $j$  belong to the same partition element  $\mathcal{B}_u$  for some  $u \in \{1, \dots, k\}$ . For example, one could take  $\mathcal{B}^{(0)} = \{\{1, \dots, p\}\}$ ,  $k = 1$ ,  $c_1 = \dots = c_p = 1$ .



2. For  $t = 2, \dots, T$ , repeat:

(a) For  $i = 1, \dots, n$  repeat:

- i. Let  $\mathcal{B}^- = (B_1^-, \dots, B_{k^-}^-)$  denote the partition of  $\{1, \dots, p\} \setminus \{i\}$  determined by the ties in the labels  $\{c_1, \dots, c_p\} \setminus \{c_i\}$  and let  $c_1^*, \dots, c_{k^-}^*$  be the unique labels among  $\{c_1, \dots, c_p\} \setminus \{c_i\}$ . For each  $u \in \{1, \dots, k^-\}$  let  $\mathcal{B}^{*u}$  denote the extension of  $\mathcal{B}^-$  to a size  $k^-$  partition of  $\{1, \dots, p\}$  obtained by adding  $i$  to the subset  $B_u^-$ . Also let  $\mathcal{B}^{**} = \mathcal{B}^- \cup \{i\}$  denote a size  $(k^- + 1)$  partition of  $\{1, \dots, p\}$  obtained by extending  $\mathcal{B}^-$  where  $i$  is placed in a singleton subset of its own.
- ii. Draw a new label  $c_i$  for index  $i$  either from  $\{c_1^*, \dots, c_{k^-}^*\} \setminus \{c_i\}$  or as a completely new and arbitrary value  $c^*$  as follows:

$$\Pr(c_i = c) \propto \begin{cases} (|B_u^-| + \rho) \times p(Y|\mathcal{B}^{*u}) & \text{if } c = c_u^*, u \in \{1, \dots, k^-\} \\ \frac{V_n(k^-+1)}{V_n(k^-)} \times p(Y|\mathcal{B}^{**}) & \text{if } c = c^* \notin \{c_1^*, \dots, c_{k^-}^*\} \end{cases}$$

(b) Set  $\mathcal{B}^{(t)} = \text{partition}(i \sim j \text{ iff } c_i = c_j)$ .

These Gibbs updates are similar to those seen for typical nonparametric Bayesian mixture models, with the important difference that calculation of the label reassignment probabilities involves evaluation of the entire marginal likelihood  $p(Y|\mathcal{B})$  for  $k^- + 1$  possible assignments of  $c_i$ . These evaluations can be time consuming unless some care is taken to streamline calculations. For example, it would be helpful to parallelize the  $k^- + 1$  calculations to multiple processors. Given the expectation that  $k^-$  would typically be quite modest, such parallelization can be accomplished on modern multicore personal computers.

The Gibbs sampler described above incrementally updates one label  $c_i$  keeping all others fixed. While such incremental updating is common to the nonparametric mixture literature, it has known limitations such as difficulty with breaking apart a prematurely formed large block. The stickiness of large blocks leads to slow mixing as one needs a large number of iterations to chip away misfit members of the large block one by one and reassemble them into a separate block. This problem is more pronounced for the MFM prior which typically discourages formation of small blocks and thus becomes more sticky when a large block forms prematurely. Merge-split samplers can overcome this problem by allowing randomly splitting one existing block into two or merging a pair (Dahl, 2003, 2005; Jain and Neal, 2004, 2007).

Traditional merge-split samplers assign items independently and with equal probability during the split process. Dahl and Newcomb (2022) introduced an adaptive procedure, known as the Sequentially Allocated Merge-Split Sampler (SAMS), which splits a large block into two by starting with a random pair as seeds for the new sub-blocks and then allocating remaining items sequentially conditional on previously allocated items. We adopt the SAMS method in our posterior sampling, where a full Gibbs scan as described earlier is interposed with five repeats of SAMS.

### 3 Hyperparameter Learning and Shrinkage

So far we have not discussed the choice of the hyperparameters in the conjugate prior specifications  $A \sim IW(\nu_0 + k + 1, A_0)$  and  $\lambda_u \sim IG((s_{0,u} + 2)/2, s_{0,u}\lambda_{0,u}/2)$ . In absence of strong prior

beliefs about model parameters, Bayesians often adopt a weakly informative prior which reduces estimation variance by inducing mild estimation bias toward a reasonable prior mean. For the inverse-Wishart part of the prior, it is quite commonplace in the literature to adopt a modest degree of freedom and a scaled identity matrix as its mean. In our context, a specific choice along this line would be

$$\nu_0 = 2, \quad A_0 = a_{00}I_k, \quad s_{0,u} = 2, \quad \lambda_{0,u} = \tau, \quad (12)$$

where  $a_{00} > 0$  is chosen in a data dependent way so that the prior mean matches the scale of the data.

Is the weakly-informative choice (12) any good? We show below and also in Section 4 that the posterior  $p(\mathcal{B}|Y)$  is quite sensitive to the choice of the hyperparameters which, as can be deduced from (5), exert a direct and great influence on the marginal likelihood  $p(Y|\mathcal{B})$ . Recall that  $p(Y|\mathcal{B})$  equals an integral of the likelihood function  $p(Y|\Gamma, \mathcal{B})$  over a  $k(k+3)/2$  dimensional space with respect to the conditional prior  $p(\Gamma|\mathcal{B})$ . Consequently, its evaluation critically depends on how the centering and the concentration of this prior distribution changes with  $k$ . We contend that for good estimation of  $\mathcal{B}$  one needs a flexible hierarchical specification so that the hyperparameters in (7) which determine the centering and the concentration of  $p(\Gamma|\mathcal{B})$  can be judiciously adjusted across various choices of  $\mathcal{B}$  in a data-dependent manner. A thorough examination of this issue is what makes our work fundamentally different from the treatment presented in [Creal and Kim \(2024\)](#).

To gain a deeper understanding of the role of the prior means  $A_0$  and  $\lambda_{0,1}, \dots, \lambda_{0,k}$ , it helps to look at the corresponding prior mean  $\Gamma_0$  of  $\Gamma$  (given a blocking structure  $\mathcal{B}$ ). From (4),  $\Gamma_0$  is a block matrix with  $k$  blocks of sizes  $p_1, \dots, p_k$ , determined by the unique elements

$$\gamma_{0,v}^2 = \frac{a_{0,uu} + (p_u - 1)\lambda_{0,u}}{p_u}, \quad \gamma_{0,uu} = \frac{a_{0,uu} - \lambda_{0,u}}{p_u}, \quad \gamma_{0,uv} = \frac{a_{0,uv}}{\sqrt{p_u p_v}}, \quad u \neq v.$$

These relations make it clear that picking a prior mean  $\Gamma_0$  may not be easy or even meaningful if one only paid attention to  $A_0$  and  $\lambda_{0,u}$ , without taking into account the block structure  $\mathcal{B}$ , especially when the blocks are of different size from one another. Seen through this lens, the weakly-informative prior in (12) does not appear a compelling choice in producing a reasonable target value  $\Gamma_0$  for  $\Gamma$ . Indeed, it gives  $\Sigma_0 = \Gamma_0 = a_{00}I_p$ , which completely ignores the block structure of the associated  $\mathcal{B}$ .

To incorporate the information in  $\mathcal{B}$  into the prior mean  $\Gamma_0$ , [Creal and Kim \(2024\)](#) recommend setting reasonable values directly for  $\Gamma_0$ . Their exact recommendation is slightly complicated, but a nearly equivalent but simplified form would be to set  $\gamma_{0,u}^2 \equiv \tau_0$ ,  $\gamma_{0,uu} = \tau_0 r_0$ , and  $\gamma_{0,uv} = 0$ ,  $u \neq v$ , where  $\tau_0 = \text{median}(S_{11}, \dots, S_{pp})$  and  $r_0 \geq 0$  is a target value for within-block correlations  $r_{uu} := \gamma_{uu}/\gamma_u^2$ . These choices translate to the following choices of the hyperparameters:

$$A_0 = \tau_0 \times \text{diag}(1 + r_0(p_1 - 1), \dots, 1 + r_0(p_k - 1)), \quad \lambda_{0,u} = (1 - r_0)\tau_0. \quad (13)$$

[Creal and Kim \(2024\)](#) recommend setting the value of  $r_0$  based on the context of the study and adopt  $r_0 = 0.35$  for their experiments and applications. Clearly, any such choice of  $r_0$  is rather ad hoc. In any given application it would be difficult to determine if  $r_0 = 0.2$  or  $r_0 = 0.5$  would have made a better choice than  $r_0 = 0.35$ . Notice that the choices described in (12) also match (13) with  $r_0 = 0$ , and hence (12) could be taken as a variant of the [Creal and Kim \(2024\)](#) prior specification. [Creal and Kim \(2024\)](#) acknowledge the difficulty in specifying a well reasoned value for  $r_0$ , and

hence recommend taking the precision parameters  $\nu_0$  and  $s_{0,u}$  to be modest, both restricted to the integers between 1 and 10, so that the ad hoc choice of  $r_0$  could be easily washed out by the information in the data.

We demonstrate here and also in Section 4 that such weakly informative priors may lead to underestimation of the block count  $k$ , thus leading to a large bias in the estimation of  $\Sigma$  in spite of the appearance of being weakly-informative for the conditional prior specifications (7) given  $\mathcal{B}$ . This bias is potentially due to the Occam’s razor property of Bayes factors (Jefferys and Berger, 1992). Recall again that the marginal likelihood  $p(Y|\mathcal{B})$  equals the integral of  $p(Y|\Gamma, \mathcal{B})$  over the  $k(k+3)/2$  free elements of  $\Gamma$  with respect to the prior on  $A$  and  $\lambda_1, \dots, \lambda_k$  where  $k = |\mathcal{B}|$ . With modest values for  $\nu_0$  and  $s_{0,u}$ , the larger the  $k$ , the smaller this integral would tend to be because the prior distribution will be more diffuse in higher dimensional spaces, even if the estimation accuracy of the corresponding posterior mean  $\Sigma_n$  did not get any worse. This phenomenon is illustrated in Figure 1 which shows the relationship between  $p(Y|\mathcal{B})$ , size of  $\mathcal{B}$ , and the estimation accuracy of  $\Sigma_n = E(\Sigma|Y, \mathcal{B})$  for one synthetic data set. It is also evident from the same figure that the performance of the weakly-informative prior remains about the same between the choices of  $r_0 = 0.35$  as in Creal and Kim (2024) and  $r_0 = 0$  as in (12). In other words, when the prior is weakly informative about  $A$  and  $\lambda_u$ , the exact information does not have a substantive impact on estimation.

An alternative to specifying weakly-informative priors is to extract some information from the data and use it to construct a data-dependent prior. An attractive choice of this type is the empirical  $g$ -prior  $p(A, \lambda_1, \dots, \lambda_k | \mathcal{B}) \propto p(Y | A, \lambda_1, \dots, \lambda_k, \mathcal{B})^g$  for a small value of  $g$ , e.g.,  $g = 1/n$ . Carvalho and Scott (2009) use a similar  $g$ -prior in a graph selection problem where it appears to offer useful regularization in sparse graph learning from limited samples. For our model, the resulting  $g$ -prior distribution is of the conjugate form as in (7) with

$$\nu_0 = 1, \quad A_0 = \frac{\sum_{i=1}^n \boldsymbol{\eta}_{i(0)} \boldsymbol{\eta}'_{i(0)}}{n}, \quad s_{0,u} = p_u - 1, \quad \lambda_{0,u} = \frac{\sum_{i=1}^n \|\boldsymbol{\eta}_{i(u)}\|^2}{n(p_u - 1)}. \quad (14)$$

Instead of fixing arbitrary prior means for  $A$  and  $\lambda_u$ , the  $g$ -prior sets the prior means in a data dependent manner. We call it an MLE-equivalent prior because the corresponding posterior mean  $E(\Sigma|Y, \mathcal{B})$  is precisely the MLE  $\hat{\Sigma}$  described in Theorem 2.1. While the MLE-equivalent prior avoids introducing bias in the estimation of  $\Sigma$  given  $\mathcal{B}$ , Figure 1 suggests it favors complex partitions, leading to severe overestimation of the number of blocks. This behavior is unsurprising because the MLE-equivalent prior clearly fails to offer any regularization against overfitting.

A more fruitful way to construct a data dependent prior is to consider an empirical or hierarchical Bayesian formulation where, instead of a single prior choice, one considers an entire family of prior distributions indexed by a small number of parameters to be estimated from the data. The advantage of such a construction is that, once these higher level parameters are estimated, calculations proceed with the corresponding element of the prior family to be used as the prior for the original analysis. The selected prior could help reduce bias as well as provide regularization much more effectively than any single prefixed prior distribution. See Efron (2019) for a thorough discussion.

For our analysis, a hierarchical framework incorporating a family of prior distributions could

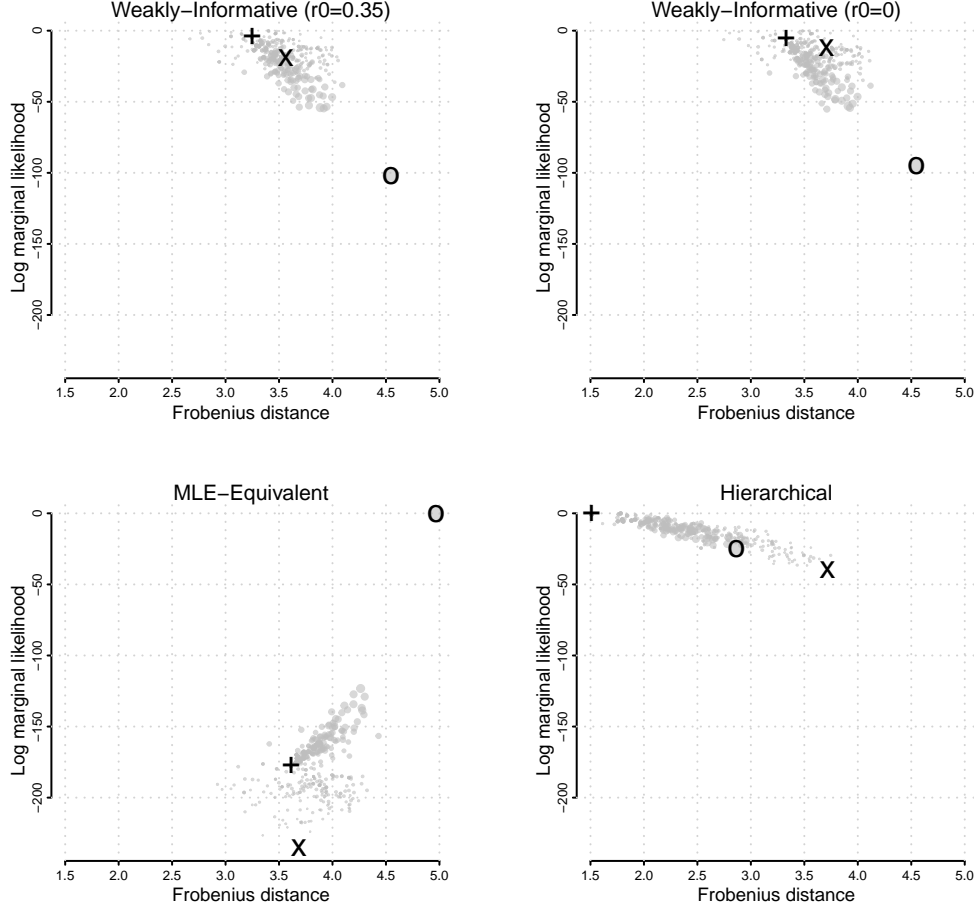


Figure 1: The effect of hyperparameter choice on the inference on  $\mathcal{B}$  and  $\Sigma$ . One synthetic dataset of size  $n = p = 20$  was generated under the group covariance matrix model assumption with  $k = 7$  and block sizes  $p_1 = 9, p_2 = 6$ , and  $p_3 = \dots = p_7 = 1$ . The marginal likelihood  $p(Y|\mathcal{B})$  (vertical axis, log scale) and the Frobenius distance (horizontal axis) between the true  $\Sigma$  and the posterior mean  $\Sigma_n = E(\Sigma|Y, \mathcal{B})$  were calculated for 200 small variations of the true partition  $\mathcal{B}$ , each variant is represented by one gray dot with the size of the dot indicating the size of the associated  $\mathcal{B}$ . The point marked "+" shows the true data generating partition  $\mathcal{B}$ , the point marked "o" shows the cluster of size 20 where each block is of size 1, and the point marked "x" shows the cluster with one block of size 20. The weakly-informative priors can be seen to favor small number of blocks even when estimation accuracy of  $\Sigma$  is relatively the same, whereas the MLE-equivalent prior clearly favors as many blocks as the number of variables. The hierarchical prior not only improves the estimation quality of  $\Sigma$  for most  $\mathcal{B}$ , it also offers a more direct relationship between the quality of  $\hat{\Sigma}$  and the corresponding  $p(Y|\mathcal{B})$ .

be constructed by considering all  $\Gamma_0$  of the form

$$\gamma_{0,u}^2 \equiv \gamma_{0,\text{variance}}^2, \quad \gamma_{0,uu} \equiv \gamma_{0,\text{within}}, \quad \gamma_{0,uv} \equiv \gamma_{0,\text{between}}, \quad u \neq v,$$

determined by three unknown scalar quantities  $\gamma_{0,\text{variance}}^2 \geq \gamma_{0,\text{within}} \geq \gamma_{0,\text{between}}$ . By (4) this imme-

diately fixes  $A_0$  and  $\lambda_{0,u}$  to be

$$\lambda_{0,u} = \gamma_{0,\text{variance}}^2 - \gamma_{0,\text{within}}, \quad a_{0,uu} = \gamma_{0,\text{variance}}^2 + (p_u - 1)\gamma_{0,\text{within}}, \quad a_{0,uv} = \gamma_{0,\text{between}}\sqrt{p_u p_v}, \quad u \neq v.$$

In other words,  $(A_0, \lambda_{0,1}, \dots, \lambda_{0,k})$  reside within a 3-dimensional subspace such that the prior mean of  $\Gamma$  is a homogeneous block covariance matrix where all block-specific variances are the same, all within-block covariances are the same, and all cross-block covariances are the same. Note that the weakly-informative choice (13) of Creal and Kim (2024) is one point within this homogeneous subspace with  $\delta_1 = \tau_0(1 - r_0)$ ,  $\delta_2 = 0$ ,  $\delta_3 = \tau_0 r_0$ . Having a homogeneous block matrix as the prior mean allows information sharing across blocks, where block-level variances and covariances for smaller blocks are shrunk more toward central values which are estimated from the data and are likely influenced more heavily by information from larger blocks. Seen through this lens, the hierarchical prior could be seen as a facilitator of estimation shrinkage – with the shrinkage target and the shrinkage intensity both learned from the data.

Toward estimating the shrinkage target and intensity, we take  $s_{0,u} \equiv s_0$ , and reparametrize  $\delta_1 = \gamma_{0,\text{variance}}^2 - \gamma_{0,\text{within}}$ ,  $\delta_2 = \gamma_{0,\text{between}}$ ,  $\delta_3 = \gamma_{0,\text{within}} - \gamma_{0,\text{between}}$ , so that

$$\lambda_{0,u} = \delta_1, \quad a_{0,uv} = \sqrt{p_u p_v} \delta_2 + 1_{u=v}(\delta_1 + p_u \delta_3), \quad (15)$$

and specify the hyper-priors  $\delta_1 \sim Ga(2, 4)$ ,  $\delta_2 \sim Ga(10, 1)$ ,  $\delta_3 \sim Ga(10, 1)$ . We also assign priors to control shrinkage intensity as  $\log(\nu_0 - 2) \sim T_1(0, 1)$ ,  $\log s_0 \sim T_1(0, 1)$ , allowing a broad range of shrinkage intensities. Posterior estimation of  $(\nu_0, s_0, \delta_1, \delta_2, \delta_3)$  can be easily performed by expanding the Markov chain Monte Carlo method described earlier; see Appendix C.

Figure 1 suggests that the hierarchical specification could be far superior to the weakly informative priors or the MLE-equivalent prior for estimating both  $\mathcal{B}$  and  $\Sigma$ . The hierarchical prior learns both the prior mean and the prior concentration for  $A$  and  $\lambda_u$  (given  $\mathcal{B}$ ) from the data and leads to much better estimates of  $\Sigma$  than the other choices. At the same time, it assigns lower marginal likelihood score  $p(Y|\mathcal{B})$  to partitions  $\mathcal{B}$  for which the associated estimate  $\Sigma_n$  is not very good. Indeed, unlike the weakly-informative or MLE-equivalent specifications, under the hierarchical setting, the magnitude of  $p(Y|\mathcal{B})$  seems much more directly related to the quality of  $\Sigma_n$  rather than simplistic features such as the size of  $\mathcal{B}$ . We show in the next section that the favorable performance of the hierarchical specification is quite typical across various data generating processes and that the resulting estimation method is an excellent candidate for high-dimensional covariance matrix estimation even when the group covariance assumption is somewhat misspecified.

## 4 Numerical Experiments

Here we report results from numerical experiments we ran to examine two key questions. When the group covariance assumption is reasonably accurate, what advantages are gained with the hierarchical prior which attempts to adaptively shrink toward a subspace of homogeneous block matrices? How good is the quality of covariance estimation when the group covariance assumption is false? In answering the first question, we compared the hierarchical prior against the weakly-informative prior of (12) which is a special case of (13) with  $r_0 = 0$  and  $\nu_0$  and  $s_0$  fixed at 2. Performance was assessed according to both statistical accuracy of the covariance estimate and correct recovery of the partition  $\mathcal{B}$ . For the second question, we examined the covariance

estimation accuracy under various alternative sparsity assumptions or other lower-dimensional structures, including block-diagonal structures, order-dependent sparsity, entrywise-independent sparsity, block-sparsity, and factor-based sparsity. For these evaluations, we compared our method against other bespoke methods such as banding, tapering, threshold-based, and Ledoit-Wolf shrinkage estimators.

#### 4.1 Impact of shrinkage on block covariance estimation

In our first experiment, we examined the relative performance of the hierarchical prior against the weakly-informative prior when the group covariance matrix assumption was correct. In generating synthetic data, we fixed the dimension  $p = 50$  and considered two possible samples sizes:  $n \in \{25, 50\}$ . Results from  $n = 25$  are presented here. See Figure 12 and Figure 13 in the Appendix for  $n = 50$ . We considered three possible maximum cluster counts  $k^* \in \{5, 10, 20\}$ . For each combination of  $(p, n, k^*)$ , we considered  $3 \times 3$  scenarios which differed from one another in terms of how the true grouped covariance matrix  $\Sigma$  was set. For each scenario, 100 replicates of  $(\mathcal{B}, \Sigma, Y)$  were generated as follows. We first generated  $\mathcal{B}$  by randomly assigning each variable  $i \in \{1, \dots, p\}$  a label  $c_i \in \{1, \dots, k^*\}$  with  $\Pr(c_i = u) \propto \max(0.1, 0.7^u)$ . This ensured that the actual cluster count  $k \leq k^*$  and the clusters were of unequal relative sizes. Next we generated  $\Sigma = P_{\mathcal{B}}\Gamma$ , where  $\Gamma$  was a block covariance matrix with  $k$  blocks which was generated according to the prior (7) with  $\nu_0$  and all  $s_{0,u}$  assigned a common value  $\tau \in \{1, 10, 100\}$  and  $A_0$  and  $\lambda_{0,u}$  set according to the hierarchical specification (15) with  $(\delta_1, \delta_2, \delta_3)$  taken to be one of the three possible configurations:

- $\delta_1 = 0.5, \delta_2 = 0, \delta_3 = 0$  (diagonal  $\Gamma_0$ ),
- $\delta_1 = 0.5, \delta_2 = 0, \delta_3 = 0.5$  (block-diagonal  $\Gamma_0$ ), or
- $\delta_1 = 0.5, \delta_2 = 0.2, \delta_3 = 0.3$  (homogeneous block  $\Gamma_0$ ).

Finally,  $Y = (\mathbf{y}_1, \dots, \mathbf{y}_n)$  was generated as  $\mathbf{y}_i \sim N(0, \Sigma)$ . Note that the three choices of  $\tau$  and three choices of  $(\delta_1, \delta_2, \delta_3)$  give rise to the  $3 \times 3$  sub-design within each  $(p, n, k^*)$  configuration of our experimental design. When the precision parameter  $\tau$  is large, the true covariance matrix  $\Sigma$  is nearly a homogeneous grouped covariance matrix. But when  $\tau = 1$  or 10,  $\Sigma$  could have fairly inhomogeneous within- and cross-block covariances as well as varying block variances.

Figure 2 provides a visual summary of the performance of block covariance estimation under the weakly-informative prior and the hierarchical prior across all designs with  $p = 50$  and  $n = 25$ . Two metrics were used to measure performance. The first measure was simply the Frobenius distance of  $\|\hat{\Sigma} - \Sigma\|_F$ , where  $\|A\|_F = (\sum_{i,j=1}^p |a_{ij}|^2)^{1/2}$ . The second measure evaluated accuracy of group allocation quantified as the Adjusted Rand Index (ARI) which measures similarity between two partitions by calculating the proportion of pairs of items that are either grouped together or separated in both partitions.

$$\text{ARI} = \frac{(p^2 - p) \sum_{i,j} (m_{ij}^2 - m_{i \cdot} m_{\cdot j}) - \sum_i (m_i^2 - m_{i \cdot}) \sum_j (m_j^2 - m_{\cdot j})}{(p^2 - p) \{ \sum_i (m_i^2 - m_{i \cdot}) + \sum_j (m_j^2 - m_{\cdot j}) \} / 2 - \sum_i (m_i^2 - m_{i \cdot}) \sum_j (m_j^2 - m_{\cdot j})} \quad (16)$$

where  $i = 1, \dots, r$ , and  $j = 1, \dots, s$ . Here,  $m_{ij}$  represents the number of common elements between group  $i$  in partition  $\mathcal{B}$  and group  $j$  in partition  $\mathcal{B}^*$ , and  $m_{i \cdot} = \sum_j m_{ij}$  and  $m_{\cdot j} = \sum_i m_{ij}$ .

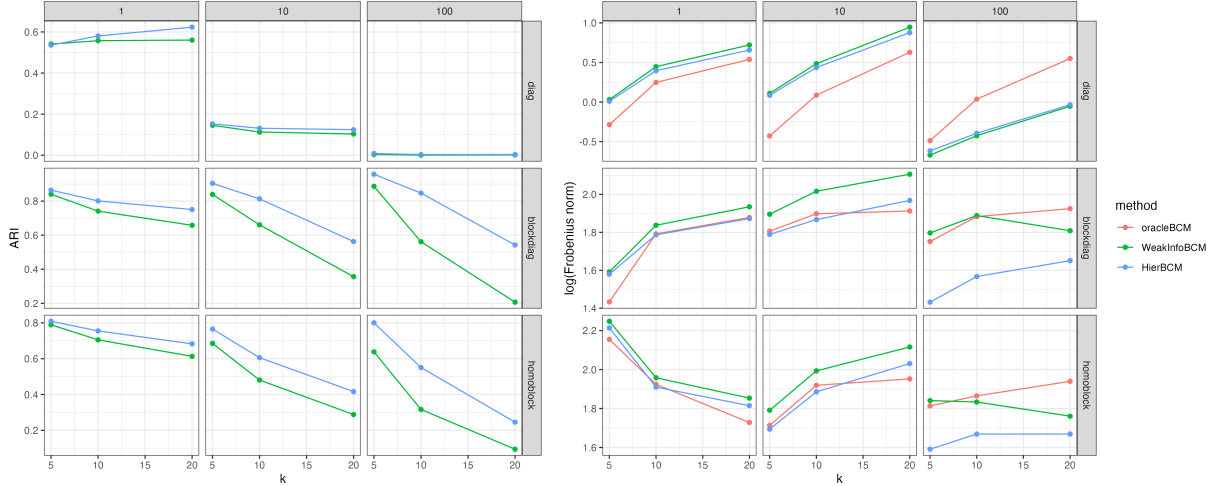


Figure 2: Estimation accuracy of different priors in the well-specified cases, measured by ARI (left) and the logarithm of Frobenius distance. Each column represents a level of precision, indicating how closely the true covariance matrix aligns with the structures shown in each row. The hierarchical prior consistently outperformed or matched the weakly-informative prior across all scenarios, benefiting from its adaptive mechanism and better clustering performance.

ARI ranges from -1 to 1, where a value of 1 indicates perfect alignment between the two partitions, while 0 suggests complete disagreement. ARI is invariant to group labels and remains robust regardless of the number of groups.

Figure 2 shows that the hierarchical prior consistently outperformed the weakly-informative prior both in terms of estimation of  $\Sigma$  and recovery of the block structure  $\mathcal{B}$ . Interestingly, it often approached or exceeded the performance of an oracle estimator of  $\Sigma$  which assumed knowledge of the true partition  $\mathcal{B}$ . Clearly, relative to the weakly-informative prior, the hierarchical prior was more adaptive across various block structures. When the true  $\Sigma$  resembled a diagonal matrix, serendipitously matching the prior mean of the weakly-informative prior in (12), the two methods performed similarly. But in all other cases, the hierarchical prior performed better, potentially due to its ability to borrow information across blocks to offer better estimates of  $\Sigma$  as well as a better scoring of  $\mathcal{B}$  through  $p(Y|\mathcal{B})$ . The larger the value of  $\tau$ , the more pronounced was this effect.

## 4.2 Broader performance analysis

In our second experiment we pitted the block covariance estimation method against a variety of covariance estimators widely used in the literature, allowing for the true covariance matrix  $\Sigma$  to deviate from the grouped covariance assumption. Again, we generated data according to the Gaussian model  $\mathbf{y}_i \sim N(0, \Sigma)$  under various assumptions on  $\Sigma$  commonly found in the literature.  $\Sigma$  remained fixed across 100 replicates for each scenario. Figure 3 shows example  $\Sigma$  matrices under each of these scenarios.

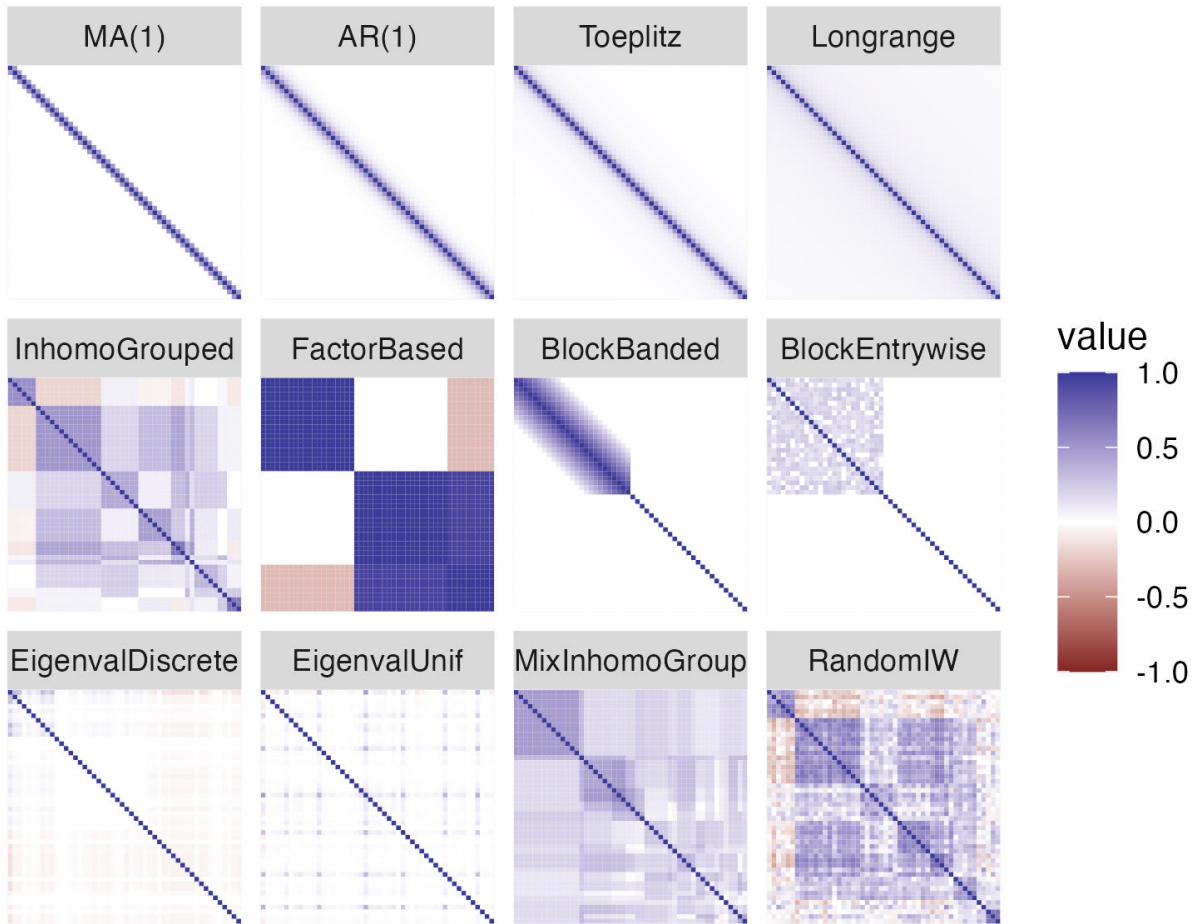


Figure 3: Example correlation matrices ( $p = 50$ ) generated for each data generating process. Each panel represents a distinct scenario, organized by the category of underlying assumptions.

#### 4.2.1 Experimental design

We considered various form of sparsity:

1. **Order-dependent sparsity**, following [Bickel and Levina \(2008\)](#) and [Cai et al. \(2010\)](#), where the covariance  $\sigma_{ij}$  decays as the distance between  $i$  and  $j$  increases. We examined four structures – MA(1), AR(1), Toeplitz, long-range dependence matrices – representing decay rates from rapid to slow. The parameters were set to  $\rho = 0.5$ ,  $H = 0.7$ , and  $\alpha = 0.3$ .



$$\text{MA(1): } \sigma_{ij} = \rho^{|i-j|} \mathbf{1}\{|i-j| \leq 1\}, \quad 1 \leq i, j \leq p \quad (17)$$

$$\text{AR(1): } \sigma_{ij} = \rho^{|i-j|}, \quad 1 \leq i, j \leq p \quad (18)$$

$$\text{Long-range: } \sigma_{ij} = \frac{1}{2}[(|i-j|+1)^{2H} - 2|i-j|^{2H} + (|i-j|-1)^{2H}], \quad 1 \leq i, j \leq p \quad (19)$$

$$\text{Toeplitz: } \sigma_{ij} = \rho|i-j|^{-(\alpha+1)}, \quad 1 \leq i, j \leq p \quad (20)$$

2. **Inhomogeneous grouped covariance matrix**, selected from a specific scenario of the grouped covariance matrix generating process described in 4.1. Specifically, we set  $k^* = p/5$ ,  $\tau = 10$ ,  $(\delta_1, \delta_2, \delta_3) = (0.5, 0.2, 0.3)$ . This inhomogeneous grouped covariance matrix was also used as the mean parameter in the inverse-Wishart distribution to generate random covariance matrices in other scenario.
3. **Factor-based sparsity**, following Zou et al. (2006), where data was generated from three latent factors:  $f_1 \sim N(0, 290)$ ,  $f_2 \sim N(0, 300)$ ,  $f_3 = -0.3f_1 + 0.925f_2 + \gamma$ ,  $\gamma \sim N(0, 1)$ , where  $f_1, f_2$ , and  $\gamma$  were independent. Observations were generated as  $Y_i = f_j + \epsilon$ , with  $\epsilon \sim N(0, 1)$ , and the proportion of  $Y_i$  drawn from  $f_1, f_2$ , and  $f_3$  were set to 40%, 40%, and 20%, respectively.
4. **Block-sparsity**, following Cai et al. (2012), where the covariance matrix  $\Sigma$  was block-diagonal:  $\Sigma = \text{diag}(A_1, A_2)$ , with  $A_1$  and  $A_2$  being  $p/2$  by  $p/2$  matrices. The first block,  $A_1$ , was diagonal with all entries set to 4. The second block,  $A_2$ , was considered under two structures: a banded matrix with entries  $\sigma_{ij} = (1 - |i-j|/10)_+$ ; entrywise-independent sparsity, where  $A_2 = B + \epsilon I$ , with  $b_{ij}$  being independently drawn from  $\text{Unif}(0.3, 0.8) \times \text{Bernoulli}(0.2)$ , and  $\epsilon = \max(\lambda_{\min}(B), 0) + 0.01$  ensuring positive definiteness.

Apart from these sparsity structures, we also considered lower-dimensional structures, following Ledoit and Wolf (2020), where covariance matrices were generated from eigen decomposition. Eigenvalues are either discrete (40%, 40%, and 20% of the eigenvalues were set to 10, 3, and 1, respectively), or uniformly distributed (eigenvalues were drawn uniformly between 1 and 10). Eigenvectors were randomly generated to form orthonormal matrices. Discrete eigenvalues tended to induce a block structure in the covariance matrices.

We also considered two other structures where the group covariance assumption is violated: (1) mixtures of block covariance matrices, where true covariance matrix was a mixture of three independently generated inhomogeneous grouped covariance matrices  $(k^*, \tau, \delta_1, \delta_2, \delta_3) = (p/5, 10, 0.5, 0.2, 0.3)$  with equal mixing weights. (2) random Inverse-Wishart distributed covariance matrices, where the true covariance matrix was drawn from  $IW(\nu_0, (\nu_0 - p - 1)\Sigma_{ig})$ , centered at the previously described inhomogeneous grouped covariance matrix  $\Sigma_{ig}$ . The precision parameter  $\nu_0$  controlled deviation from the group structure assumption, and we set  $\nu_0 = p + 2$ .

To facilitate comparison among different estimators and data generating processes, we used the sample covariance matrix as a benchmark, assessing performance by the ratio of the Frobenius norm of each estimator to that of the sample covariance matrix:

$$\mathbf{R}_{est/sample} = \frac{\|\hat{\Sigma} - \Sigma\|_F}{\|S - \Sigma\|_F}. \quad (21)$$

A lower ratio indicates better estimator performance, with a ratio of 1 suggesting similar performance to the sample covariance matrix.

#### 4.2.2 Competing estimators

We considered block covariance matrix estimators under three priors: weakly-informative, MLE-equivalent, and our proposed hierarchical prior. Each Bayesian method ran 5000 MCMC iterations, discarding the first 500 as burn-in, and every fifth posterior sample retained. The posterior mean served as the estimator for Bayesian methods.

For alternative covariance estimators, we utilized methods available in the R package `cvCovEst` (Boileau et al., 2022), which can be categorized based on their underlying assumptions:

- order-dependent sparsity: Banding (Bickel and Levina, 2008) and tapering estimators (Cai et al., 2010) assumes that covariance decays with distance between variable indexes.
- order-invariant sparsity: hard thresholding (Bickel and Levina, 2008), SCAD thresholding, and adaptive LASSO estimators (Zou, 2006; Rothman et al., 2009) assume sparsity without dependence on variable ordering.
- shrinkage estimators: Ledoit-Wolf linear and nonlinear shrinkage estimators do not impose structural assumptions but shrink sample eigenvalues toward a target. (Ledoit and Wolf, 2004, 2020).

Banding estimator applies hard thresholds to off-diagonal entries of sample covariance matrix based on variables' distance, setting distant covariances to zero. Tapering estimator gradually shrinks off-diagonal entries with increasing distance, resulting in a dense matrix with diminishing covariances. Hard thresholding and SCAD estimator apply thresholds to individual entries of the sample covariance matrix. Adaptive LASSO estimator penalizes entries unequally using data-dependent weights. Ledoit-Wolf linear shrinkage applies uniform shrinkage to all sample eigenvalues, pulling them toward a central value, while the nonlinear shrinkage estimator adjusts the shrinkage intensity based on the distribution of the sample eigenvalues, allowing for individualized shrinkage.

#### 4.2.3 Comparison of estimators across various covariance structures

We examined the performance of different estimators under various covariance structures using  $p = 20, 50^1$ , and  $p/n = 0.1, 1, 1.25, 2$ . For clear comparison, we grouped alternative estimators by underlying assumptions and selected the best-performing one from each category.

In Figure 4, the block covariance estimator using the hierarchical prior (lavender line) and weakly-informative prior (blue line) generally outperformed alternative estimators, except in cases involving order-dependent structures with rapidly decaying dependencies and randomly generated Inverse-Wishart covariances. This result highlighted the adaptability of the group covariance matrix assumption across diverse covariance types. Notably, the hierarchical prior consistently surpassed the weakly-informative prior, demonstrating its capacity to flexibly accommodate different structural patterns in the data.

---

<sup>1</sup>See Figure 14 for case  $p = 20$  in the Appendix.

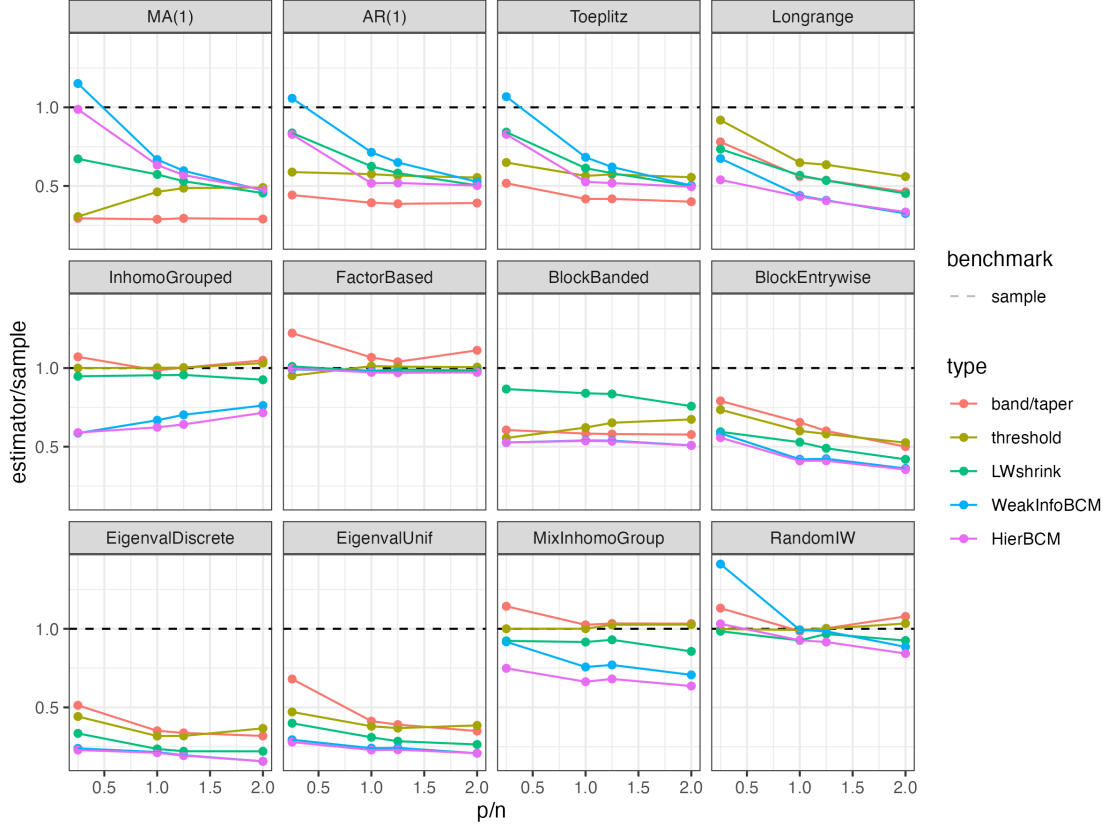


Figure 4: Comparison of estimation accuracy among different covariance estimators across various covariance structures ( $p = 50$ ). The block covariance estimator with the hierarchical prior (lavender line) generally outperformed alternative estimators, except in cases with order-dependent structures featuring rapidly decaying dependencies. This result underscored the adaptability of the block structure assumption across diverse covariance types. In addition, the hierarchical prior consistently surpassed both the weakly informative prior and the sample covariance matrix.

For covariance with order-dependent sparsity, the banding/tapering estimator consistently performed better than other estimators, except in cases with long-range dependencies. This is because the banding/tapering estimator correctly bet on the underlying structure, whereas other estimators struggled due to misspecification. Moving from left to right across the first row of panels, as dependency decayed more slowly, covariance matrices had less sparsity and larger off-diagonal values (as shown in Figure 3). In such cases, the assumptions underlying the banding/tapering and thresholding estimators became less appropriate, the block covariance estimator performed better, particularly as long-range dependencies grew stronger.

For random Inverse-Wishart distributed covariance matrices, our estimator with a hierarchical prior performed comparable to, or outperformed, the best alternative (namely, the Ledoit-Wolf shrinkage estimator in cases where  $p/n = 0.1$ ). In contrast, the weakly-informative prior often performed worse than, or on par with, the sample covariance when  $p \leq n$ . This might be attributed to the lack of clear structure in randomly generated matrices (see Figure 3), which deviated from group covariance matrix and sparsity assumptions. Unlike the hierarchical prior, the

weakly-informative prior lacked adaptivity, making it less robust against misspecification.

Across all scenarios, our estimator outperformed the sample covariance matrix. Notably, the weakly-informative prior sometimes underperformed relative to the sample covariance matrix, particularly when  $n > p$  and for Inverse-Wishart or rapidly decaying, order-dependent structures. This result illustrated the limitations of a fixed shrinkage target and the necessity of adjustable shrinkage intensity. The hierarchical prior provided adaptability in shrinkage, ensuring robust performance even under challenging conditions.

## 5 Relation to Other Covariance Estimation Methods

Stochastic block covariance estimation is inherently a regularized factor model, enforcing identical factor loadings within the same cluster. It also inherits the rationale behind Stein’s class of shrinkage estimators, which reduces the dispersion of sample eigenvalues through clustering. Discussing clustered factor model and Stein’s estimators can mirror stochastic block covariance estimation from different perspectives, enhancing our understanding on how it achieves strong performance across various covariance structures.

### 5.1 Clustered factor model

A natural alternative for representing block covariance matrices is the clustered factor model (Taylor-Rodríguez et al., 2017; Tong and Hansen, 2023). Suppose  $\mathbf{y}_i \stackrel{\text{i.i.d.}}{\sim} N(\mathbf{0}, \Sigma)$ , where  $\Sigma$  is a block covariance matrix as defined in equation (1). The data can be modeled using a latent factor model:

$$\mathbf{y}_i = L\mathbf{f} + \mathbf{e}_i, \tag{22}$$

where  $\mathbf{y}_i$  is a  $p \times 1$  vector,  $L$  is a  $p \times r$  matrix of factor loadings,  $\mathbf{f}$  is a  $r \times 1$  vector of latent factors with  $E(\mathbf{f}) = \mathbf{0}$ , and  $\text{cov}(\mathbf{f}) = I_r$ , and  $\mathbf{e}_i \stackrel{\text{i.i.d.}}{\sim} N(\mathbf{0}, E)$  is the error term with  $E$  being a diagonal matrix. The covariance matrix can then be expressed as

$$\Sigma = LL^T + E, \tag{23}$$

with factor loadings identical for variables within the same block.

The block covariance matrix has several advantages over the clustered factor model. First, block covariance models are more general, as the clustered factor model only represents a subset of block covariance matrices that are positive definite (see Theorem 1 and Lemma 1 in Tong and Hansen (2023)). Second, clustered factor models require  $k \times r + r$  parameters, where  $r$  is the number of factors, leading to higher parameter complexity unless the block covariance matrix is highly parsimonious ( $k < 2r - 3$ ). Third, clustered factor model requires selecting an appropriate number of factors, and the number of factors is bound by the covariance structure, posing a great challenge in model estimation. One might consider an infinite factor model and introduce a prior to truncate it to a finite number (Bhattacharya and Dunson, 2011). However, undoubtedly, estimating the number of factors would introduce additional complexity and computational burden for block covariance estimation. Additionally, block covariance models are more straightforward

and transparent for interpretation, as latent factors and their loadings can often be challenging to interpret meaningfully.

## 5.2 Stein’s class of shrinkage estimators

Upon revisiting the numerical experiment results shown in Figures 4 and Figure 14, the consistently good performance of the Ledoit-Wolf shrinkage estimator captured our attention. The Ledoit-Wolf shrinkage estimator consistently ranked as the second-best method, following closely behind the block covariance matrix estimator in most cases, except for those involving banded/tapered or sparse banded structures. It outperformed or remained competitive with the block covariance estimators when the true covariance matrix was generated from an inverse-Wishart distribution or followed an MA(1) or AR(1) process in settings where  $n > p$ . Notably, it consistently surpassed the sample covariance matrix even in challenging cases.

The Stein’s class of shrinkage estimators, originally introduced by Stein (1975, 1986), shrinks the sample eigenvalues while retaining the sample eigenvectors. The rationale behind this approach is that sample eigenvalues tend to be more dispersed than population eigenvalues, and appropriate shrinkage can improve estimation accuracy. Let  $S$  denote the sample covariance matrix with eigen decomposition  $S = U\Lambda U'$ . Stein’s shrinkage estimators take the form

$$\hat{\Sigma} = U\Delta U', \tag{24}$$

where  $U$  represent the eigenvector of  $S$ , and  $\Delta = \text{diag}(\delta_1, \dots, \delta_p)$  consists of modified sample eigenvalues, where each  $\delta_j$  is a function of the sample eigenvalues  $\Lambda$ , i.e.,  $\delta_j = \varphi_j(\Lambda)$ , mapping from the positive diagonal matrix to itself.

A key development in extending Stein’s estimator to high dimensional settings stems from advances in random matrix theory, particularly the Marčenko-Pastur equation (Wigner, 1955; Marčenko and Pastur, 1967; Silverstein, 1995). Building upon these fundamental results, various nonlinear shrinkage estimators have been developed, with the Ledoit-Wolf shrinkage estimators (Ledoit and Wolf, 2022) being notable examples.

The block covariance estimator shares some conceptual similarities with Stein’s estimators, since both reduce the dispersion of sample eigenvalues, albeit through different mechanisms. While Stein’s approach shrinks eigenvalues directly, guided by the rotation of the sample eigenvectors, the block covariance estimator achieves shrinkage by clustering eigenvalues, driven by a block-sparse rotation, effectively eliminating within-group variance.

We compared the performance of block covariance estimator against various shrinkage estimators within Stein’s family, including the population eigenvalues plug-in estimator ( $\Delta = \Lambda$ ), Finite Sample OPTimal estimator (Ledoit and Wolf, 2012) ( $\delta_j = u_j' \Sigma u_j$ ), and the analytical nonlinear Ledoit-Wolf estimator (Ledoit and Wolf, 2020). Our numerical experiments focused on cases where  $p > n$ , with  $p/n = 1.1, 2, 5, 10$ . We followed the same data generating processes described in Section 4.2.3, except that the factor-based sparsity scenario was replaced with a degenerate covariance matrix where all eigenvalues were equal to 1.

Figure 5 displays a comparison of estimation accuracy between block covariance estimator (BCM) and Stein’s class of estimators across various covariance structures. <sup>1</sup> The block covari-

---

<sup>1</sup>To prevent numerical instability in density estimation, we truncated sample eigenvalues below  $10^{-8}$  to zero when applying the Ledoit-Wolf method.

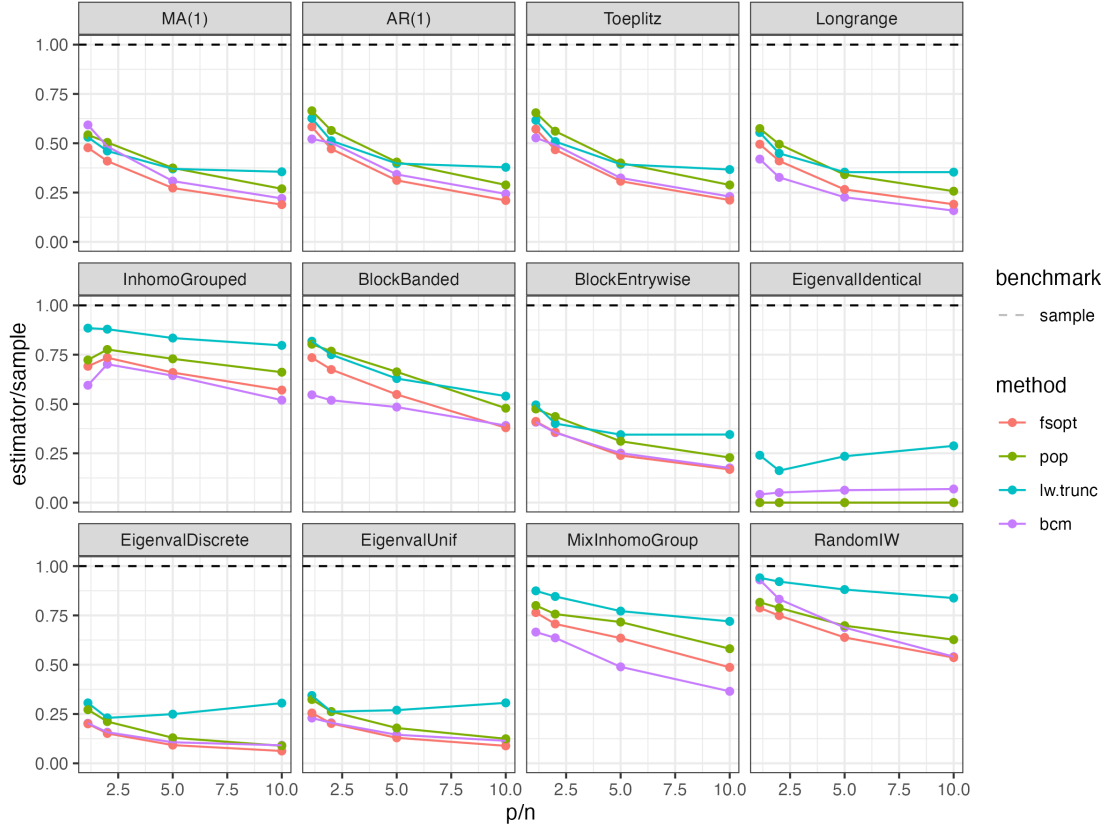


Figure 5: Comparison of estimation accuracy of block covariance estimation with Stein’s class of shrinkage estimators across various covariance structure ( $p = 50$ ). The block covariance estimator generally outperformed or was comparable to oracle estimators, except in cases where the true covariance matrix followed an MA(1) process or a random inverse-Wishart distribution.

ance estimators generally outperformed or was comparable to the oracle estimators, except when the covariance matrix was generated from an MA(1) process (characterized by rapid decay in dependency) or a random inverse-Wishart distribution. Across nearly all scenarios, the block covariance estimator consistently surpassed Ledoit-Wolf estimator. This advantage arose from the BCM’s reliance on rotation learning, which effectively leveraged structural information within the data, allowing better adaptation when such structure was present. In contrast, Stein’s family estimators operated without strong structural assumptions, making them overly conservative and limiting their flexibility and adaptability to various covariance matrix configurations.

The block covariance estimator and Stein’s estimator originate from two classical models: factor analysis and principle component analysis (PCA), respectively. Our model introduces additional regularization on factor loadings by enforcing identical factor loadings within the same cluster while also promoting sparsity. Similar extensions of factor analysis and PCA can be found in [Rohe and Zeng \(2023\)](#), where varimax rotation is recommended to promote sparsity and interpretability for non-Gaussian data.

## 6 Application

### 6.1 Neural coordination

Previous studies (Caruso et al., 2018; Jun et al., 2022; Schmehl et al., 2024; Chen et al., 2024) have shown that individual neurons can encode two simultaneously presented stimuli through a turn-taking dynamics called "code juggling", where neurons randomly switch between two composite stimuli either at a slow rate across trials or at a fast rate within a trial. However, this alternation between stimuli is not entirely random. Some evidence suggests a coordinated pattern of code juggling across neural populations (Jun et al., 2022; Schmehl et al., 2024). This coordination can be represented by a block structure in covariance matrices, which may provide valuable insights into how neural circuits contribute to perception and behavior, a fundamental question in neuroscience.

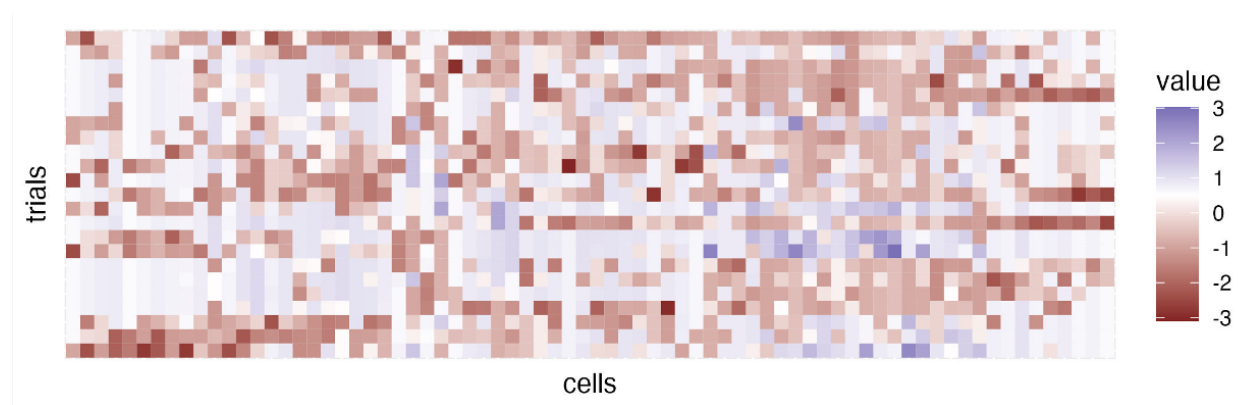


Figure 6: Score matrix of 74 neurons across 23 trials, with each entry showing the neuron’s tendency to encode stimulus A (blue) or B (red) during simultaneous dual-stimulus exposure. Co-fluctuating and oppositely fluctuating patterns among neurons suggest clustering in the covariance structure.

We analyze a dataset from Ruff and Cohen (2016), where monkeys performed a motion direction change detection task while neural activity was recorded. In trials involving dual stimuli (A and B), adjacent drifting Gabor patches with different orientations were presented. In single stimulus trials, only one of the constituent drifting Gabor patches was visible. A multi-electrode array is planted in V1 area recording spike activities of 101 neurons simultaneously. We use a subset of the data and preprocess it to generate a score matrix for 74 neurons across 23 trials, where each entry reflects a neuron’s inclination to encode stimulus A. For a detailed description of the preprocessing procedure, refer to Appendix F.1.

Figure 6 displays the score matrix, organized according to clustering from our block covariance matrix estimator. It reveals distinct clusters of neurons with different patterns in their activity fluctuations. Our primary focus is on examining the block structure of the covariance matrix underlying these fluctuations. Figure 7 and 8 show the posterior mean of covariance matrices and posterior similarity matrices, which represent the posterior probability of two neurons being clustered together. Neurons are sorted based on the clustering results from the weakly informative prior to facilitate comparison.

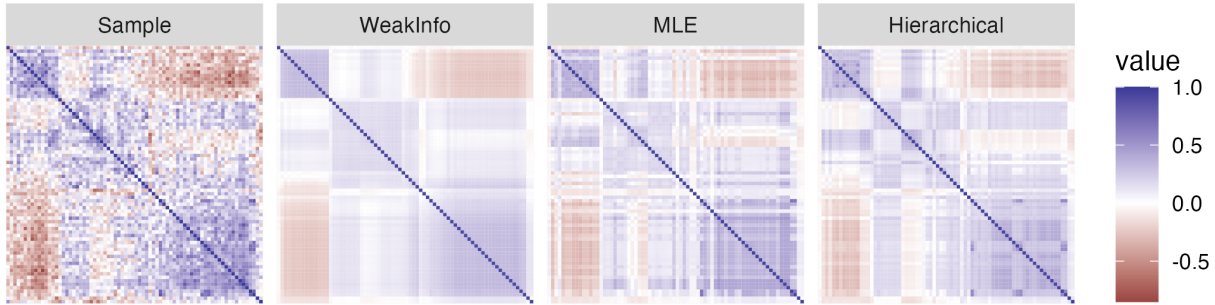


Figure 7: Posterior mean of covariance matrices under different priors in the neural population coordination application. The weakly informative prior oversimplifies the block structure and misrepresents between-block covariances, while the MLE-equivalent prior favors sparsity, resulting in many isolated small-sized blocks. The hierarchical prior, with adaptive shrinkage, refines the block structure to better reflect the underlying data.

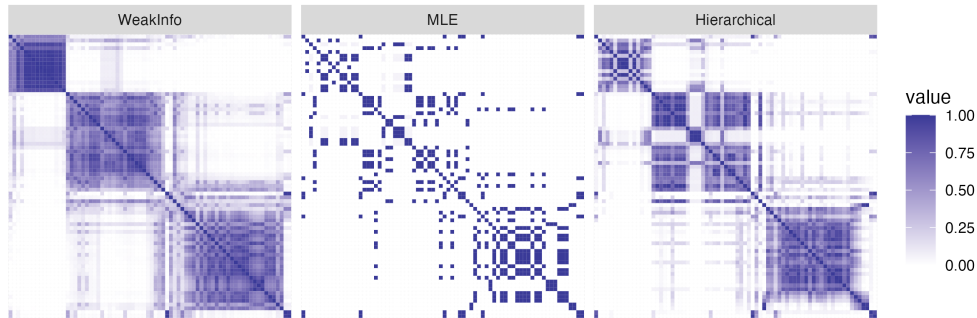


Figure 8: Posterior similarity matrices under different priors. The weakly informative prior oversimplifies the block structure, failing to capture finer details. The MLE-equivalent prior exhibits slow MCMC mixing or may become trapped in a local mode, affecting accurate block identification.

In Figure 7, three primary clusters emerge: a median-sized cluster of 15 neurons and two larger clusters of around 26 and 33 neurons. Neurons within the first cluster are highly interconnected, positively correlated with the second cluster and negatively correlated with the third.

The weakly informative prior excessively shrinks the covariance toward a block diagonal structure, oversimplifying the block structure and misrepresenting between-block covariances. As shown in Figure 7, the weakly informative prior manifests two main issues in covariance estimation: (1) diminished within-block covariance, where some high positive within-block covariances among certain neurons are significantly reduced due to the shrinkage. (2) a reversal of the sign of between-block covariance, where some negative covariances between the second and third clusters are shrunk to weak positive covariances. These issues are reflected in its underlying block assignments, which are primarily influenced by within-block covariances and fail to account for the heterogeneity in between-block covariances. For instance, Figure 7 reveals a subgroup of neurons



in the second block that are positively correlated with the first block and negatively correlated with the third block, while other neurons in the second block display the opposite pattern. However, this nuanced sub-block structure is not clearly captured by the weakly informative prior, as seen in the posterior similarity matrix in Figure 8.

The MLE-equivalent prior focuses on capturing the sparsity of the sample covariance matrix, resulting in the formation of too many blocks, particularly isolated small-sized ones. In Figure 7, the numerous white ribbons in the covariance estimator indicate that many entries are overly shrunk toward zero, especially within small blocks. Comparing the posterior similarity matrix in Figure 8 with the sample covariance matrix in Figure 7, it appears that the MLE-equivalent prior prioritizes sparsity over preserving the block structure. The block assignment is largely driven by its sparsity, rather than by meaningful block patterns. Additionally, the posterior similarity matrix of the MLE-equivalent prior shows a concentrated distribution, which may suggest slow MCMC mixing or a tendency to get stuck in a local mode.

Both the weakly informative and MLE-equivalent priors suffer from the mis-specification of the shrinkage target and lack adaptive intensity. In contrast, the hierarchical prior refines the block structure to better align with the data through adaptive shrinkage. As seen in Figure 7, the hierarchical prior is sensitive to the heterogeneity of between-block covariances, capturing a more detailed and accurate structure than the weakly informative prior. For instance, it effectively captures sub-block structures within the second and third large blocks. Unlike the MLE-equivalent prior, the hierarchical prior avoids introducing isolated small blocks and excessive shrinkage toward zero, providing a smoother, more accurate estimator. Figure 8 further illustrates how the hierarchical prior enhances cluster segmentation and restores essential features. This refined block structure affirms the presence of coordination within the neural population, providing a clear depiction of potential neural circuits.

## 6.2 Monthly stock returns of energy and financial companies

Estimating the covariance matrix is a critical aspect of the financial market, particularly in the realms of portfolio optimization and risk management. Covariance, which gauges the co-movements of returns across diverse assets, forms the basis for comprehending the relationships between these assets. Through an accurate covariance-based classification, investors can gain insights into the interconnections among different assets, facilitating portfolio diversification to mitigate specific risks.

To underscore the importance of covariance structure, we reference a concise example from [Liechty et al. \(2004\)](#). In this example, we examine monthly stock returns spanning April 1996 to December 2001 for nine companies (68 time points). These companies belong to either the energy sector (Reliant, Chevron, British Petroleum, and Exxon) or the finance sector (Citi-Bank, Lehman Brothers, Merrill Lynch, and Bank of America). Notably, Enron underwent a transformation from an energy company to a finance company in the 1990s and subsequently declared bankruptcy in December 2001. In our analysis, we focus solely on data prior to Enron's bankruptcy, differing from the analysis presented in [Liechty et al. \(2004\)](#).

We aim to: (1) cluster these nine companies to assess whether their equity variations align with their industrial classifications, and (2) evaluate Enron's transition from the energy sector to the finance sector prior to its bankruptcy. Given the significant fluctuations in some stocks, assuming a block structure in the correlation matrix is more appropriate. Therefore, we apply our estimator

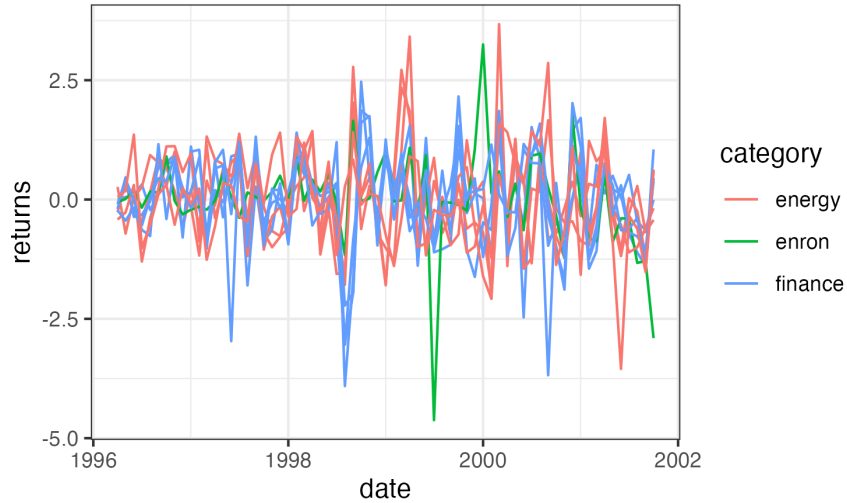


Figure 9: Monthly returns of Enron and other energy and finance companies.

to the standardized data .

Figure 9 displays a trace plot of standardized monthly returns, presenting a challenge to discern whether Enron’s fluctuations are more in sync with finance or energy companies. The block covariance estimation, shown in Figure 10, reveals three main clusters: Enron and Reliant (energy), other energy companies, and finance companies. These classification align with their respective industrial classifications.

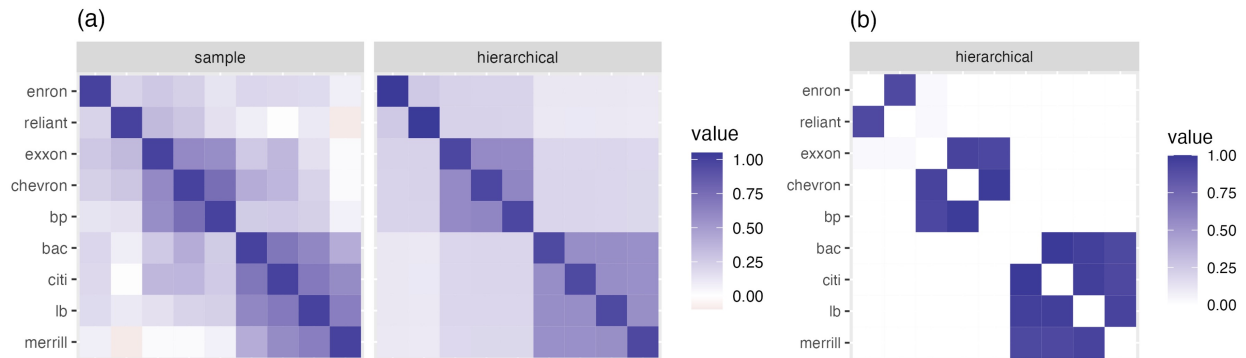


Figure 10: Estimators of covariance matrix (left: sample covariance, right: block covariance under the hierarchical prior) and Posterior similarity matrix. Enron behaves more closely resembles that of energy companies than finance companies.

It appears that Enron did not successfully transition from the energy sector to finance, as its behavior more closely resembles that of energy companies than finance companies. Enron and Reliant share similarities, exhibiting lower covariance with other energy companies and finance companies compared to the remaining energy companies. This finding is consistent with the conclusion of [Liechty et al. \(2004\)](#), which also indicated Enron’s unsuccessful transition.

### 6.3 Phenotypic integration of Mediterranean shrubs under contrasting environmental conditions

The analysis of correlation structures among traits provides insight into phenotypic integration, which refers to "the pattern of functional, developmental, and/or genetic correlation among different traits in a given organism" (Pigliucci, 2003). Traits may be positively or negatively correlated depending on their functional roles, influencing how organisms adapt to varying environmental conditions. To examine phenotypic integration under different environmental conditions, we analyze the correlation matrices of 20 ecophysiological traits in Mediterranean shrub samples (*Lepidium subulatum* L., Brassicaceae) grown under both stressful (drought) and favorable conditions. This dataset allows us to assess differences in phenotypic integration between these environments. The experimental details are described in [Matesanz et al. \(2021\)](#).

The dataset is aggregated at the family level, where we computed the average trait values for each population and maternal family. After removing missing cases, we obtained 45 samples from plants grown under drought conditions and 55 from those in favorable conditions. To better meet the normality assumptions, we applied logarithmic or square-root transformations to most traits before standardization. The 20 traits can be categorized into the following functional groups:

- Morphological traits: specific leaf area (SLA), leaf area (LA), leaf length (LL), total estimated leaf area (TELA), plant height (PH)
- Physiological traits: midday photochemical efficiency of PSII (FvFm), relative growth rate (RGR)
- Phenological traits: onset of flower bud formation (FBF), onset of flowering (FL), onset of fruiting (FR), percentage of senescent leaves (Sen)
- Allocation traits: root-to-leaf ratio (R.L), leaf-to-stem ratio (L.S), above-ground biomass (AB), total biomass (TB)
- Reproductive traits: number of inflorescences (IN), inflorescence size (IS), number of flowers (FN), reproductive output (RO), seed size (SS)

These traits may either compete for resources or work together in a coordinated manner.

Figure 11 presents the sample correlation matrices and their posterior mean estimates under favorable and stressful conditions. The overall block structure aligns well with functional group classifications. Notably, reproductive traits (IS, FN, IN, RO) exhibit strong positive correlations, reflecting coordinated investment in reproduction. Similarly, phenological traits (FR, FBF, FL) form a highly correlated cluster. These traits occur in sequence during the reproductive timeline, which explains their strong correlation. The morphological traits (LA, LL, PH, TELA) are positively correlated with above-ground biomass (AB), indicating an integrated response to plant growth. Additionally, a cross-functional cluster emerges, incorporating physiological (RGR, FvFm), allocation (R.L, TB), phenological (Sen), and reproductive (SS) traits.

Under drought conditions, the correlation matrix exhibits enhanced correlation across functional groups compared to the favorable environment. (1) Stronger negative correlations between reproductive phenology (FBF, FL, FR) and other traits. (2) Greater positive correlations between reproductive traits (IS, FN, IN, RO) and traits in the cross-functional group (Sen, R.L, TB, FvFm,

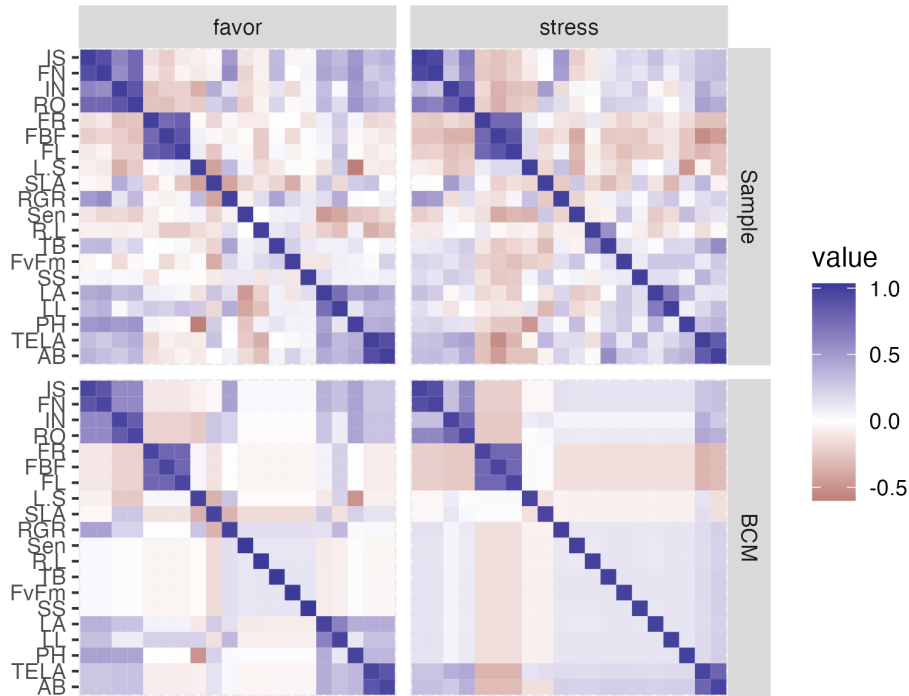


Figure 11: Posterior mean of covariance matrices of traits under favorable and stressful environments. The overall block structure aligns well with functional group classifications, with notable differences in correlation patterns across environments. Under drought conditions, cross-functional correlations strengthen, suggesting an adaptive response to environmental stress.

SS). (3) Enhanced positive correlations between above-ground growth traits (LA, LL, PH, TELA, AB) and traits in the cross-functional group (Sen, R.L, TB, FvFm, SS).

This pattern is consistent with a drought-escape strategy (Blanco-Sánchez et al., 2022; Matesanz et al., 2020), wherein plants accelerate reproductive timing and enhance growth to complete life cycle before drought conditions become more severe. For example, a larger cross-functional cluster emerge, involving coordinated changes in physiological, phenological, and allocation traits. Under drought conditions, plants that begin reproduction earlier tend to grow larger (higher PH, TB, LA), produce larger seeds, show increased leaf senescence, and exhibit higher growth rates and photochemical efficiency.

Matesanz et al. (2021) quantified phenotypic integration in plants by counting the number of significantly nonzero pairwise correlations between traits and found that plants under stressful conditions exhibit higher phenotypic integration. In our model, this increased integration appears as a reduction in the number of distinct trait clusters (see posterior similarity matrix in Figure 19 for a clear block assignment). Under drought conditions, traits from different functional groups that are only weakly or negatively associated in favorable conditions become more strongly or positively associated, suggesting an adaptive reconfiguration of trait relationships to cope with environmental stress.

## 7 Discussion

We introduced a stochastic block structure for covariance matrix estimation, motivated by practical demands in real-world applications. Beyond its interpretability, the stochastic block structure effectively reduces dimensionality, while being more general, flexible, and efficient compared to conventional sparsity assumptions or shrinkage estimators. The block structure also offers greater adaptability across different types of covariance matrices, enhancing its utility in various fields.

In many practical applications, the block structure may be more relevant for the correlation matrix than the covariance matrix. For example, principle component analysis and copula models rely on correlation matrices. In portfolio selection, some assets may exhibit large variances, which can dominate clustering results and obscure important co-movements. When clustering is performed based on the covariance matrix, variables with large variances often form distinct blocks, pushing variables with smaller variances into a single block. This sensitivity to variance can lead to suboptimal clustering that fails to capture meaningful patterns of co-fluctuation.

To more accurately capture the block structure in a correlation matrix, we recommend standardizing the data to have zero mean and unit variance before applying the block covariance model. However, standardizing data is not always feasible, as block correlation matrices may be an intermediate product rather than the target estimator. Furthermore, standardization can ignore the uncertainty quantification of variance estimation by treating variance as fixed. A more direct approach is to consider a canonical representation of block correlation matrices. However, this introduces computational challenges due to the inherent restriction that correlation  $r_{ij} \in [-1, 1]$ , which imposes constraints on the parameters  $(A, \lambda)$ . These constraints make it difficult to apply standard techniques, as a conjugate prior is not readily available, complicating both the estimation of correlations and the block assignment process.

A better solution might involve introducing scaling parameters to account for heteroskedasticity. We can express the covariance matrix as  $\Sigma = S^{1/2}\Sigma S^{1/2}$ , where  $S$  is a diagonal matrix representing individual variances, and  $\Sigma$  is a block covariance matrix.

One of the main challenges of our method is the computational burden, especially for large datasets where the number of variables  $p$  exceeds 200, as often encountered in proteomics, gene expression, and finance. The bottleneck lies in estimating the block assignments, where even with an effective merge-split sampler (Dahl and Newcomb, 2022), we encounter slow mixing and high computational costs.

Several strategies could improve computational efficiency. One solution is to enhance the Metropolis Hasting proposal in the sampler. Currently, the sampler is constrained to move between  $K + 1$  (split) and  $K - 1$  (merge) clusters. For  $K - 1$  cases, there is only one way to merge, while for  $K + 1$  cases, the splitting depends on the previous allocated items, which may be inefficient. A more flexible proposal could be constructed by leveraging clustering structures from previous samples, potentially based on the posterior similarity matrix. Another approach, inspired by Duan and Bhattacharya (2024), is to construct a graph where each node represents a potential state, and then perform MCMC using random walks over the graph. By optimizing the graph's nodes and edges, larger jumps toward more likely structures can be achieved, improving the efficiency of the sampling process. However, designing this graph and understanding its theoretical properties require careful consideration, as the effectiveness of this method depends on how well the graph structure reflects the underlying block structure and ensures adequate exploration of the posterior distribution.

Instead of focusing on improving the sampler itself, we could explore parallelizing the sampling process to alleviate the computational burden. A well-known approach involves divide-and-conquer (D&C) strategies ([Sivaganesan et al., 2017](#); [Chang and Fisher, 2013](#); [Ni et al., 2019](#); [Lovell et al., 2018](#); [Srivastava et al., 2015](#); [Campbell and Broderick, 2019](#)), which divide the problem into simpler, independent components that are processed in parallel, and then combine the results to approximate the full solution. Unlike the traditional D&C methods, which break down large-scale data problems into small datasets, we break down the variables themselves, with some variables appearing across multiple subsets to serve as benchmarks. Each subset of data can be modeled independently, and the posterior samples can be "sutured" together based on the clustering information provided by these benchmark variables. Determining how to appropriately divide the variables and merge the posterior samples to obtain a reliable and effective approximation of the target estimator requires careful planning and methodological considerations.

## References

- Andrieu, C. and J. Thoms (2008). A tutorial on adaptive mcmc. *Statistics and computing* 18, 343–373.
- Antoniak, C. E. (1974). Mixtures of dirichlet processes with applications to bayesian nonparametric problems. *The Annals of Statistics* 2(6), 1152–1174.
- Archakov, I. and P. R. Hansen (2024). A canonical representation of block matrices with applications to covariance and correlation matrices. *Review of Economics and Statistics* 106(4), 1099–1113.
- Bhattacharya, A. and D. B. Dunson (2011). Sparse bayesian infinite factor models. *Biometrika* 98(2), 291–306.
- Bickel, P. J. and E. Levina (2008). Regularized estimation of large covariance matrices. *The Annals of Statistics* 36(1), 199–227.
- Blanco-Sánchez, M., M. Ramos-Muñoz, B. Pías, J. A. Ramírez-Valiente, L. Díaz-Guerra, A. Escudero, and S. Matesanz (2022). Natural selection favours drought escape and an acquisitive resource-use strategy in semi-arid mediterranean shrubs. *Functional Ecology* 36(9), 2289–2302.
- Boileau, P., N. S. Hejazi, M. J. van der Laan, and S. Dudoit (2022). Cross-validated loss-based covariance matrix estimator selection in high dimensions. *Journal of Computational and Graphical Statistics* 0, 1–12.
- Cai, T. T., Z. Ren, and H. H. Zhou (2016). Estimating structured high-dimensional covariance and precision matrices: Optimal rates and adaptive estimation. *Electronic Journal of Statistics* 10(1), 1 – 59.
- Cai, T. T., M. Yuan, et al. (2012). Adaptive covariance matrix estimation through block thresholding. *The Annals of Statistics* 40(4), 2014–2042.
- Cai, T. T., C.-H. Zhang, and H. H. Zhou (2010). Optimal rates of convergence for covariance matrix estimation. *The Annals of Statistics* 38(4), 2118–2144.
- Campbell, T. and T. Broderick (2019). Automated scalable bayesian inference via hilbert coresets. *Journal of Machine Learning Research* 20(20), 1–38.
- Caruso, V. C., J. T. Mohl, C. Glynn, J. Lee, S. M. Willett, A. Zaman, A. F. Ebihara, R. Estrada, W. A. Freiwald, S. T. Tokdar, et al. (2018). Single neurons may encode simultaneous stimuli by switching between activity patterns. *Nature communications* 9(1), 1–16.
- Carvalho, C. M. and J. G. Scott (2009). Objective bayesian model selection in gaussian graphical models. *Biometrika* 96(3), 497–512.
- Chang, J. and J. W. I. Fisher (2013). Parallel sampling of dp mixture models using sub-cluster splits. In *Advances in Neural Information Processing Systems*, pp. 620–628.

- Chen, Y., J. M. Groh, and S. T. Tokdar (2024). Spike count analysis for multiplexing inference (scampi).
- Creal, D. and J. Kim (2024). Bayesian estimation of cluster covariance matrices of unknown form. *Journal of Econometrics* 241(1), 105725.
- Dahl, D. B. (2003). An improved merge-split sampler for conjugate dirichlet process mixture models. *Technical Report 1*, 086.
- Dahl, D. B. (2005). Sequentially-allocated merge-split sampler for conjugate and nonconjugate dirichlet process mixture models. *Journal of Computational and Graphical Statistics* 11(6), 4–2.
- Dahl, D. B. and S. Newcomb (2022). Sequentially allocated merge-split samplers for conjugate bayesian nonparametric models. *Journal of Statistical Computation and Simulation* 92(7), 1487–1511.
- Duan, L. L. and A. Bhattacharya (2024). Graph-accelerated markov chain monte carlo using approximate samples.
- Efron, B. (2019). Bayes, oracle bayes and empirical bayes. *Statistical science* 34(2), 177–201.
- Fan, J., Y. Liao, and H. Liu (2016). An overview of the estimation of large covariance and precision matrices. *The Econometrics Journal* 19(1), C1–C32.
- Ferguson, T. S. (1973). A bayesian analysis of some nonparametric problems. *The Annals of Statistics* 1(2), 209–230.
- Jain, S. and R. M. Neal (2004). A split-merge markov chain monte carlo procedure for the dirichlet process mixture model. *Journal of computational and Graphical Statistics* 13(1), 158–182.
- Jain, S. and R. M. Neal (2007). Splitting and merging components of a nonconjugate dirichlet process mixture model. *Bayesian Analysis* 2(3), 445–472.
- Jefferys, W. H. and J. O. Berger (1992). Ockham’s razor and bayesian analysis. *American scientist* 80(1), 64–72.
- Jun, N. Y., D. A. Ruff, L. E. Kramer, B. Bowes, S. T. Tokdar, M. R. Cohen, and J. M. Groh (2022). Coordinated multiplexing of information about separate objects in visual cortex. *Elife* 11, e76452.
- Kingman, J. F. (1978). The representation of partition structures. *Journal of the London Mathematical Society* 2(2), 374–380.
- Ledoit, O. and M. Wolf (2004). A well-conditioned estimator for large-dimensional covariance matrices. *Journal of multivariate analysis* 88(2), 365–411.
- Ledoit, O. and M. Wolf (2012). Nonlinear shrinkage estimation of large-dimensional covariance matrices. *The Annals of Statistics* 40(2), 1024–1060.



- Ledoit, O. and M. Wolf (2020). Analytical nonlinear shrinkage of large-dimensional covariance matrices. *The Annals of Statistics* 48(5), 3043–3065.
- Ledoit, O. and M. Wolf (2022). The power of (non-) linear shrinking: A review and guide to covariance matrix estimation. *Journal of Financial Econometrics* 20(1), 187–218.
- Lee, C. and D. J. Wilkinson (2019). A review of stochastic block models and extensions for graph clustering. *Applied Network Science* 4(1), 1–50.
- Liechty, J. C., M. W. Liechty, and P. Müller (2004). Bayesian correlation estimation. *Biometrika* 91(1), 1–14.
- Lovell, G., R. P. Adams, and S. Byrne (2018). Distributed bayesian nonparametric clustering via parallelized gibbs sampling. *Journal of Machine Learning Research* 19(26), 1–29.
- Marčenko, V. A. and L. A. Pastur (1967). Distribution of eigenvalues for some sets of random matrices. *Mathematics of the USSR-Sbornik* 1, 457–483.
- Matesanz, S., M. Blanco-Sánchez, M. Ramos-Muñoz, M. de la Cruz, R. Benavides, and A. Escudero (2021). Phenotypic integration does not constrain phenotypic plasticity: differential plasticity of traits is associated to their integration across environments. *New Phytologist* 231(6), 2359–2370.
- Matesanz, S., M. Ramos-Muñoz, M. Blanco-Sánchez, and A. Escudero (2020). High differentiation in functional traits but similar phenotypic plasticity in populations of a soil specialist along a climatic gradient. *Annals of Botany* 125(6), 969–980.
- Miller, J. W. and M. T. Harrison (2018). Mixture models with a prior on the number of components. *Journal of the American Statistical Association* 113(521), 340–356.
- Ni, G., J. Li, and L. Zhang (2019). A parallel mcmc method for large-scale nonparametric mixture models. *Bayesian Analysis* 14(1), 41–67.
- Perrot-Dockes, M., C. Lévy-Leduc, and L. Rajjou (2022). Estimation of large block structured covariance matrices: Application to ‘multi-omic’ approaches to study seed quality. *Journal of the Royal Statistical Society Series C: Applied Statistics* 71(1), 119–147.
- Pigliucci, M. (2003). Phenotypic integration: studying the ecology and evolution of complex phenotypes. *Ecology letters* 6(3), 265–272.
- Pitman, J. (2006). *Combinatorial stochastic processes: Ecole d’été de probabilités de saint-flour xxxii-2002*. Springer.
- Pitman, J. and M. Yor (1997). The two-parameter poisson-dirichlet distribution derived from a stable subordinator. *Ann. Probab.* 25(4), 855–900.
- Pourahmadi, M. (2013). *High-dimensional covariance estimation: with high-dimensional data*, Volume 882. John Wiley & Sons.

- Rajaratnam, B., H. Massam, and C. M. Carvalho (2008). Flexible covariance estimation in graphical Gaussian models. *The Annals of Statistics* 36(6), 2818 – 2849.
- Rohe, K. and M. Zeng (2023, 07). Vintage factor analysis with varimax performs statistical inference. *Journal of the Royal Statistical Society Series B: Statistical Methodology* 85(4), 1037–1060.
- Rothman, A. J., E. Levina, and J. Zhu (2009). Generalized thresholding of large covariance matrices. *Journal of the American Statistical Association* 104(485), 177–186.
- Ruff, D. A. and M. R. Cohen (2016). Attention increases spike count correlations between visual cortical areas. *Journal of Neuroscience* 36(28), 7523–7534.
- Schmehl, M. N., V. C. Caruso, Y. Chen, N. Y. Jun, S. M. Willett, J. T. Mohl, D. A. Ruff, M. Cohen, A. F. Ebihara, W. A. Freiwald, et al. (2024). Multiple objects evoke fluctuating responses in several regions of the visual pathway. *Elife* 13, e91129.
- Silverstein, J. W. (1995). Strong convergence of the empirical distribution of eigenvalues of large-dimensional random matrices. *Journal of Multivariate Analysis* 55, 331–339.
- Sivaganesan, S., R. Natarajan, and S. Rao (2017). Scalable bayesian nonparametric clustering via parallelization. *Journal of Computational and Graphical Statistics* 26(2), 436–447.
- Srivastava, R., J. Li, and D. B. Dunson (2015). Scalable bayes via barycenter in wasserstein space. *Journal of the American Statistical Association* 110(512), 1458–1472.
- Stein, C. (1975). Estimation of a covariance matrix. Rietz Lecture, 39th Annual Meeting IMS, Atlanta, Georgia, 28 August 1975.
- Stein, C. (1986). Lectures on the theory of estimation of many parameters. *Journal of Soviet Mathematics* 34, 1373–1403.
- Taylor-Rodríguez, D., K. Kaufeld, E. M. Schliep, J. S. Clark, and A. E. Gelfand (2017). Joint Species Distribution Modeling: Dimension Reduction Using Dirichlet Processes. *Bayesian Analysis* 12(4), 939 – 967.
- Tong, C. and P. R. Hansen (2023). Characterizing correlation matrices that admit a clustered factor representation. *Economics Letters* 233, 111433.
- Wigner, E. P. (1955). Characteristic vectors of bordered matrices with infinite dimensions. *The Annals of Mathematics* 62, 548–564.
- Wu, W. B. and M. Pourahmadi (2003). Nonparametric estimation of large covariance matrices of longitudinal data. *Biometrika* 90(4), 831–844.
- Zou, H. (2006). The adaptive lasso and its oracle properties. *Journal of the American statistical association* 101(476), 1418–1429.
- Zou, H., T. Hastie, and R. Tibshirani (2006). Sparse principal component analysis. *Journal of computational and graphical statistics* 15(2), 265–286.

## Supplementary Materials

### A Obtain rotation matrix $Q$

$$Q^{(p_k)} = \tilde{Q}^{(p_k)} \begin{pmatrix} 1/\sqrt{p_k} & & & & & \\ & 1/\sqrt{1+1^2} & & & & \\ & & \ddots & & & \\ & & & 1/\sqrt{i+i^2} & & \\ & & & & \ddots & \\ & & & & & 1/\sqrt{(p_k-1)+(p_k-1)^2} \end{pmatrix} \quad (25)$$

$$\tilde{Q}^{(p_k)} = (\tilde{Q}_1^{(p_k)} \tilde{Q}_{-1}^{(p_k)}) = \begin{pmatrix} 1 & -1 & 1 & 1 & \cdots & 1 \\ 1 & 0 & -2 & 1 & \cdots & 1 \\ 1 & 0 & 0 & -3 & \ddots & 1 \\ 1 & 0 & 0 & 0 & \ddots & 1 \\ 1 & 0 & 0 & 0 & \cdots & -(p_k-1) \\ 1 & 1 & 1 & 1 & \cdots & 1 \end{pmatrix} \quad (26)$$

### B Proof of Theorem 2.1

From Theorem 3 in [Archakov and Hansen \(2024\)](#), we have maximum likelihood estimator for  $A$  and  $\lambda_k$  ( $k \in \{1, \dots, K\}$ ) as

$$\hat{A} = \frac{\sum_{i=1}^n \boldsymbol{\eta}_{i(0)} \boldsymbol{\eta}'_{i(0)}}{n}, \quad \hat{\lambda}_k = \frac{\sum_{i=1}^n \boldsymbol{\eta}'_{i(k)} \boldsymbol{\eta}_{i(k)}}{n(p_k-1)} \quad (9)$$

Since  $\Sigma$  is a rotation of  $D$ , the MLE of  $\Sigma$  is obtained by plugging  $\hat{A}$  and  $\hat{\lambda}_k$  into equation (3).

$$\hat{\Sigma} = Q \hat{D} Q' = Q \begin{pmatrix} \hat{A} & 0 & \cdots & 0 \\ 0 & \hat{\lambda}_1 I_{p_1-1} & \ddots & \vdots \\ \vdots & \ddots & \ddots & 0 \\ 0 & \cdots & 0 & \hat{\lambda}_K I_{p_K-1} \end{pmatrix} Q' \quad (27)$$

Recall the equations (4), we can represent entries of  $\Sigma$  using entries of  $A$  and  $\lambda_k$  as follows:

$$\sigma_k^2 = \frac{a_{kk} + (p_k - 1)\lambda_k}{p_k}, \quad \sigma_{kk} = \frac{a_{kk} - \lambda_k}{p_k}, \quad \sigma_{kl} = \frac{a_{kl}}{\sqrt{p_k p_l}} \quad (28)$$

Plugging equation (6) to equation (28), we have

$$\hat{\sigma}_k^2 = \frac{1}{np_k} \sum_{i=1}^n (\eta_{i(0),k}^2 + \boldsymbol{\eta}'_{i(k)} \boldsymbol{\eta}_{i(k)}) \quad (29)$$

$$\hat{\sigma}_{kk} = \frac{1}{np_k} \sum_{i=1}^n (\eta_{i(0),k}^2 - \frac{1}{p_k - 1} \boldsymbol{\eta}'_{i(k)} \boldsymbol{\eta}_{i(k)}) \quad (30)$$

$$\hat{\sigma}_{kl} = \frac{1}{n\sqrt{p_k p_l}} \sum_{i=1}^n \boldsymbol{\eta}'_{i(0),k} \boldsymbol{\eta}_{i(0),l} \quad (31)$$

Let  $\tilde{\mathbf{y}}_i$  denotes  $i^{th}$  observation, which is a sorted  $p \times 1$  vector. We have  $\tilde{\mathbf{y}}_i = (\tilde{\mathbf{y}}_i^{(p_1)'}, \dots, \tilde{\mathbf{y}}_i^{(p_K)'})'$ , where  $\tilde{\mathbf{y}}_i^{(p_k)}$  is a  $p_k \times 1$  data vector which belongs to block  $k$ . Consequently, We can partition  $Q' \tilde{\mathbf{y}}_i$  as follows:

$$Q' \tilde{\mathbf{y}}_i = (Q_1^{(p_1)'} \tilde{\mathbf{y}}_i^{(p_1)}, \dots, Q_1^{(p_K)'} \tilde{\mathbf{y}}_i^{(p_K)}, Q_{-1}^{(p_1)'} \tilde{\mathbf{y}}_i^{(p_1)}, \dots, Q_{-1}^{(p_K)'} \tilde{\mathbf{y}}_i^{(p_K)}) \quad (32)$$

Notice  $Q' \tilde{\mathbf{y}}_i = \boldsymbol{\eta}'_i = (\boldsymbol{\eta}'_{i(0)}, \boldsymbol{\eta}'_{i(1)}, \dots, \boldsymbol{\eta}'_{i(k)}, \dots, \boldsymbol{\eta}'_{i(K)})$ ,  $\boldsymbol{\eta}_{i(0)} \in \mathbb{R}^{K \times 1}$ , and  $\boldsymbol{\eta}_{i(k)} \in \mathbb{R}^{(p_k-1) \times 1}$ . Then we have

$$\begin{aligned} \boldsymbol{\eta}'_{i(0)} &= (Q_1^{(p_1)'} \tilde{\mathbf{y}}_i^{(p_1)}, \dots, Q_1^{(p_K)'} \tilde{\mathbf{y}}_i^{(p_K)}) \\ \boldsymbol{\eta}'_{i(k)} &= Q_{-1}^{(p_k)'} \tilde{\mathbf{y}}_i^{(p_k)}, \quad k \in \{1, \dots, K\} \end{aligned} \quad (33)$$

Plug equations (33) into equations (29)-(31), we can directly match the MLE of  $\Sigma$  back to MLE of pairwise covariance.

$$\begin{aligned} \hat{\sigma}_k^2 &= \frac{1}{np_k} \sum_{i=1}^n \mathbf{y}_i^{(k)'} Q^{(p_k)} Q^{(p_k)'} \mathbf{y}_i^{(k)} = \frac{1}{np_k} \sum_{i=1}^n \mathbf{y}_i^{(k)'} \mathbf{y}_i^{(k)} = \frac{1}{np_k} \sum_{i=1}^n \sum_{j \in \mathcal{B}_k} y_{ij}^2 \\ \hat{\sigma}_{kk} &= \frac{1}{np_k} \sum_{i=1}^n (\mathbf{y}_i^{(k)'} Q_1^{(p_k)} Q_1^{(p_k)'} \mathbf{y}_i^{(k)} - \frac{1}{(p_k - 1)} \mathbf{y}_i^{(k)'} Q_{-1}^{(p_k)} Q_{-1}^{(p_k)'} \mathbf{y}_i^{(k)}) \\ &= \frac{1}{np_k(p_k - 1)} \sum_{i=1}^n \mathbf{y}_i^{(k)'} \left( \frac{1}{p_k} \mathbf{1}\mathbf{1}' - \frac{1}{p_k - 1} (I - \frac{1}{p_k} \mathbf{1}\mathbf{1}') \right) \mathbf{y}_i^{(k)} \\ &= \frac{1}{np_k(p_k - 1)} \sum_{i=1}^n \mathbf{y}_i^{(k)'} (\mathbf{1}\mathbf{1}' - I) \mathbf{y}_i^{(k)} = \frac{1}{np_k(p_k - 1)} \sum_{i=1}^n \sum_{j, j' \in \mathcal{B}_k, j \neq j'} y_{ij} y_{ij'} \\ \hat{\sigma}_{kl} &= \frac{1}{np_k p_l} \sum_{i=1}^n \mathbf{y}_i^{(k)'} Q_1^{(p_k)} Q_1^{(p_l)'} \mathbf{y}_i^{(l)} = \frac{1}{np_k p_l} \sum_{i=1}^n \mathbf{y}_i^{(k)'} \mathbf{1}\mathbf{1}' \mathbf{y}_i^{(l)} = \frac{1}{np_k p_l} \sum_{i=1}^n \sum_{j \in \mathcal{B}_k, j' \in \mathcal{B}_l} y_{ij} y_{ij'} \end{aligned}$$

## C Expanded MCMC for the hierarchical method

Let  $\theta$  denote the hyperparameters  $(\nu_0, s_0, \delta_1, \delta_2, \delta_3)$ . We adopt a block-update strategy, dividing the sampling process into three major steps:

Start with initial values  $\mathcal{B}^{(0)}$  and  $\theta^{(0)}$ , for each iteration  $t \in \{1, \dots, T\}$ :

1. Given  $(\theta^{(t-1)})$ , update  $\mathcal{B}^{(t)}$  using the Sequentially Allocated Merge-Split Sampler (SAMS) introduced by [Dahl and Newcomb \(2022\)](#).
2. Given  $(\mathcal{B}^{(t)}, A^{(t)}, \lambda^{(t)})$ , update  $\theta^{(t)}$  using the Adaptive Metropolis algorithm with global adaptive scaling according to Algorithm 4 from [Andrieu and Thoms \(2008\)](#).

Once samples of  $(\mathcal{B}, \theta)$  are drawn from the posterior, those of  $\Gamma$  could be drawn easily by using the conjugate form described in [\(8\)](#).

## D Extra figures for Numerical Experiments

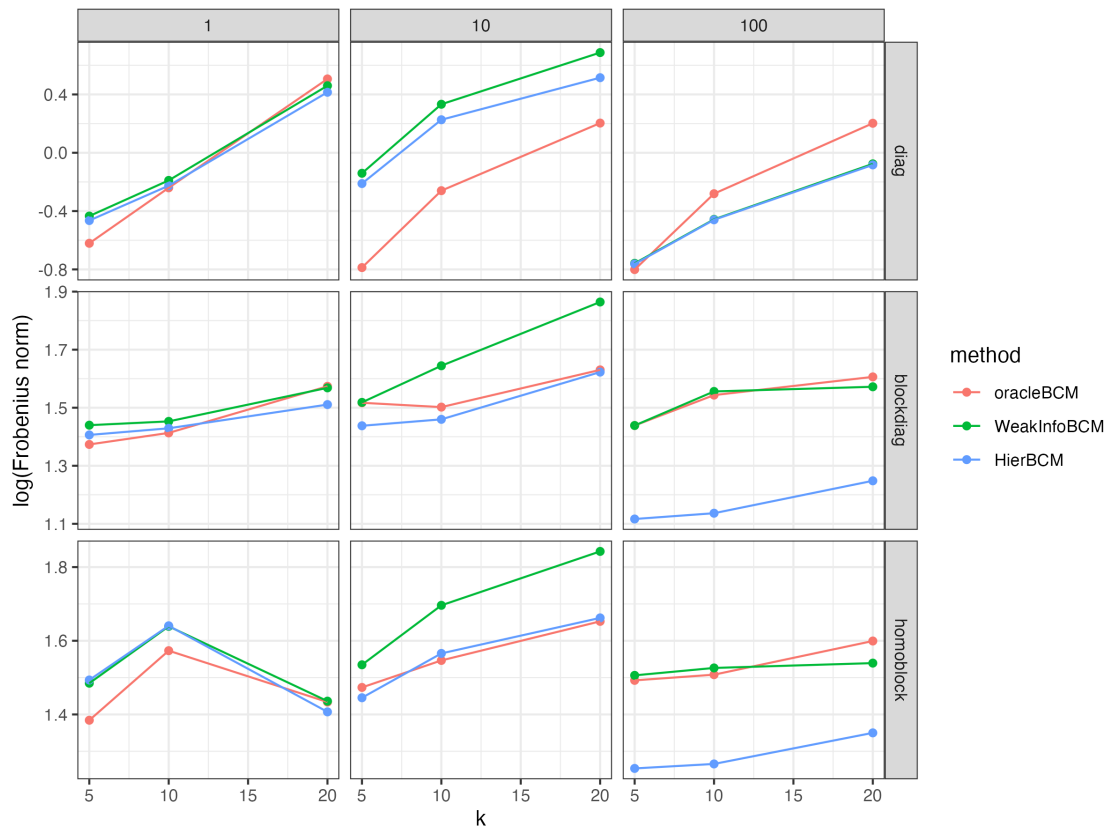


Figure 12: Comparison of estimation accuracy among different priors under well-specified cases ( $p = 50$ ).

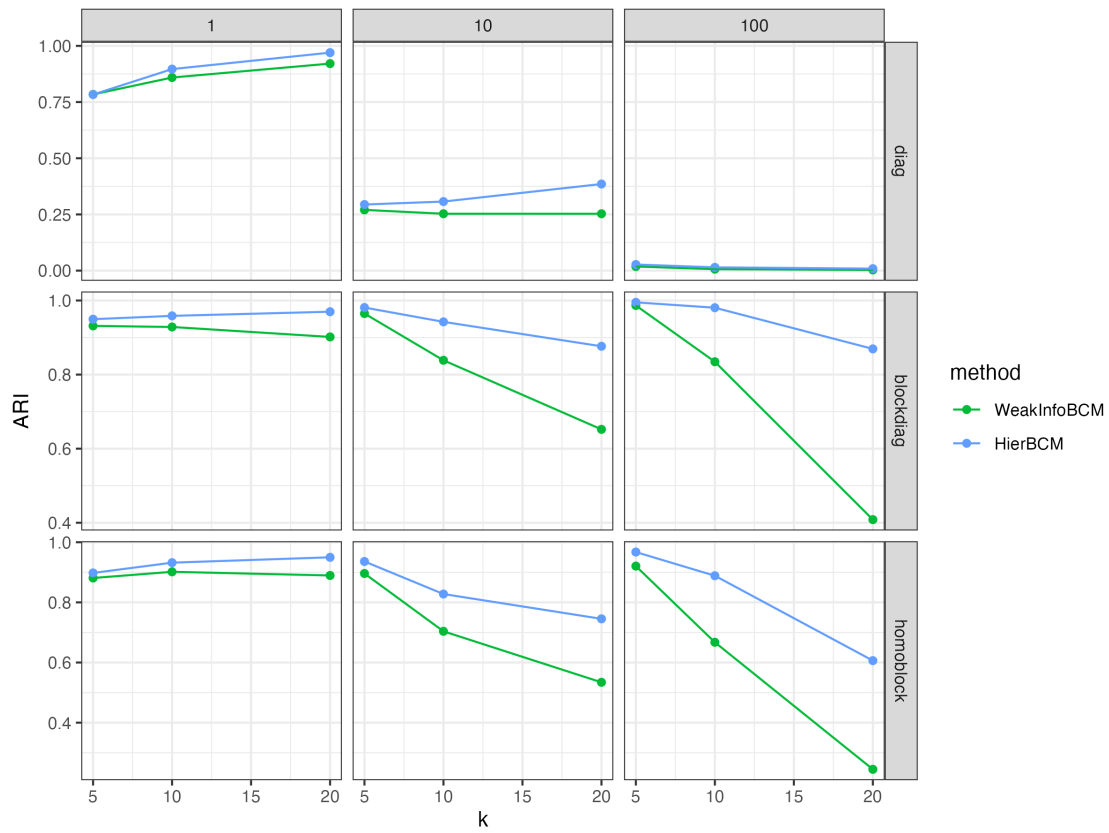


Figure 13: Comparison of clustering performance among different priors under well-specified cases ( $n = 50$ ).

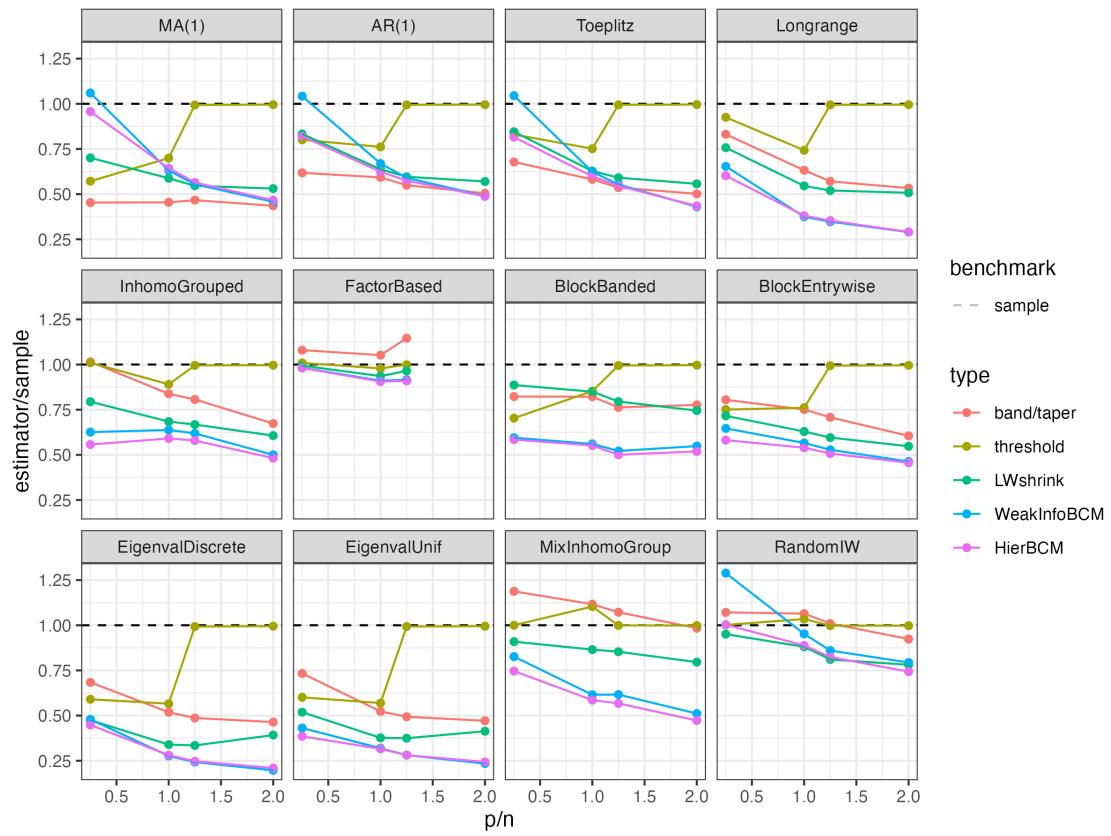


Figure 14: Estimation accuracy of different estimators across various covariances



## E Extra tables for Numerical Experiments

Table 1 present a summary statistics (posterior mean of Frobenius distance, number of blocks, ARI, R2) calculated from posterior samples. Notice R2 is a metric measuring clustering accuracy proposed by [Creal and Kim \(2024\)](#), as defined below:

$$R_2 = E(L(\hat{\Pi}, \Pi_0)) = E\left(-\frac{1}{p^2} \sum_{i=1}^p \sum_{i'=1}^p \pi_{0,ii'} \log(\hat{\pi}_{ii'})\right) \quad (34)$$

where  $\hat{\Pi}, \Pi_0$  represent estimator and the true probability matrix respectively. Each entry  $\hat{\pi}_{ii'}, \pi_{0,ii'}$  of the matrix  $\hat{\Pi}, \Pi_0$  quantify the probability individual  $i$  and  $i'$  belong to the same cluster. We consider ARI instead of R2 since R2 is sensitive to number of clusters and size of clusters. We can observe some cases that better estimation on number of blocks does not appear to be better in the performance measured by R2. R2 is not consistent with the  $\hat{K}$ .

Table 1: Comparison of priors in well-specified scenarios

Dataset	n	Prec	k	Sample	Oracle	Weak	BCM	K_Weak	K_BCM	ARI_Weak	ARI_BCM	R2_Weak	R2_BCM
diagonal	1		5	4.725	0.751	1.031	1.01	3.735	4.198	0.541	0.536	0.257	0.101
			10	4.288	1.282	1.563	1.486	6.31	7.298	0.557	0.58	0.174	0.099
			20	3.952	1.713	2.057	1.929	10.648	12.649	0.56	0.623	0.22	0.065
	25	10	5	4.895	0.652	1.116	1.09	2.153	2.835	0.145	0.153	0.145	0.145
			10	5.132	1.091	1.623	1.546	2.499	3.493	0.113	0.131	0.12	0.099
			20	5.233	1.875	2.576	2.405	3.548	5.142	0.103	0.124	0.139	0.091
	100		5	5.218	0.614	0.511	0.539	1.212	1.823	0.004	0.008	0.017	0.066
			10	5.101	1.037	0.654	0.674	1.189	1.762	0.001	0.003	0.014	0.044
			20	5.164	1.734	0.948	0.966	1.237	1.906	0.002	0.004	0.008	0.028
	1		5	3.568	0.537	0.648	0.628	4.274	4.653	0.784	0.783	0.066	0.059
			10	3.541	0.786	0.827	0.798	8.201	8.951	0.859	0.897	0.019	0.016
			20	5.15	1.659	1.584	1.514	14.939	16.052	0.921	0.97	0.002	0.001
	50	10	5	3.304	0.455	0.869	0.81	2.343	3.241	0.27	0.294	0.148	0.151
			10	3.592	0.771	1.395	1.254	3.306	5.023	0.253	0.307	0.152	0.123
			20	3.61	1.226	1.988	1.674	4.849	8.952	0.253	0.385	0.147	0.106
	100		5	3.64	0.449	0.468	0.466	1.195	1.715	0.018	0.027	0.056	0.06
			10	3.624	0.755	0.633	0.631	1.207	1.831	0.006	0.014	0.026	0.051
			20	3.612	1.224	0.927	0.92	1.247	2.043	0.003	0.009	0.016	0.036
blockdiag	1		5	8.328	4.193	4.911	4.852	4.379	4.715	0.84	0.864	0.028	0.023
			10	9.434	6.002	6.281	5.973	6.757	7.741	0.741	0.801	0.096	0.034
			20	9.51	6.543	6.922	6.504	10.801	12.981	0.658	0.75	0.104	0.026
	25	10	5	10.453	6.087	6.657	5.986	3.978	4.74	0.839	0.904	0.016	0.027
			10	10.785	6.672	7.513	6.47	4.926	6.984	0.661	0.813	0.058	0.028
			20	10.216	6.772	8.219	7.16	5.182	8.515	0.357	0.563	0.107	0.038
	100		5	10.314	5.764	6.032	4.187	4.093	4.979	0.887	0.958	0.043	0.012
			10	10.686	6.574	6.61	4.793	3.846	6.878	0.562	0.847	0.024	0.022
			20	10.319	6.854	6.102	5.212	3.296	7.029	0.207	0.543	0.024	0.023
	1		5	9.437	3.949	4.22	4.08	4.624	4.905	0.931	0.95	0.008	0.012
			10	6.854	4.109	4.275	4.175	8.451	9.1	0.929	0.959	0.006	0.006
			20	6.548	4.825	4.799	4.53	14.433	16.211	0.902	0.97	0.006	0.004
	50	10	5	7.587	4.559	4.565	4.211	4.655	4.981	0.965	0.981	0.002	0.004
			10	7.317	4.491	5.178	4.306	6.215	8.413	0.839	0.942	0.004	0.007
			20	7.61	5.106	6.451	5.067	7.74	13.082	0.652	0.876	0.03	0.009
	100		5	7.402	4.215	4.215	3.054	4.782	5.051	0.987	0.995	0.002	0.003
			10	7.494	4.681	4.74	3.116	5.322	8.431	0.835	0.981	0.001	0.001
			20	7.326	4.984	4.817	3.484	4.826	11.138	0.408	0.869	0.014	0.003
centerblock	1		5	41.761	8.625	9.467	9.149	4.207	4.594	0.789	0.809	0.069	0.045
			10	10.466	6.851	7.084	6.752	6.666	7.555	0.705	0.755	0.075	0.05
			20	9.423	5.63	6.382	6.139	10.08	11.855	0.613	0.683	0.096	0.037
	25	10	5	10.214	5.548	5.996	5.442	3.488	4.365	0.685	0.765	0.046	0.056
			10	10.772	6.815	7.339	6.591	3.942	5.498	0.481	0.606	0.061	0.052
			20	10.317	7.043	8.296	7.62	4.58	6.655	0.288	0.416	0.103	0.059
	100		5	10.685	6.132	6.301	4.91	3.144	4.384	0.638	0.8	0.04	0.045
			10	10.575	6.454	6.256	5.306	2.669	4.773	0.317	0.551	0.036	0.057
			20	10.418	6.956	5.817	5.307	2.24	4.225	0.095	0.246	0.025	0.038
	1		5	7.513	3.992	4.414	4.453	4.509	4.813	0.881	0.898	0.023	0.028
			10	7.064	4.821	5.151	5.158	8.255	8.949	0.902	0.932	0.01	0.009
			20	6.14	4.194	4.204	4.084	14.29	15.864	0.89	0.95	0.018	0.012
	50	10	5	7.563	4.364	4.64	4.243	4.313	4.842	0.896	0.936	0.006	0.015
			10	7.553	4.695	5.453	4.786	5.205	7.293	0.704	0.828	0.04	0.05
			20	7.673	5.221	6.313	5.27	6.851	11.927	0.534	0.745	0.054	0.027
	100		5	7.589	4.448	4.509	3.502	4.201	4.967	0.921	0.967	0.008	0.008
			10	7.427	4.517	4.601	3.545	3.986	6.814	0.667	0.889	0.007	0.01
			20	7.329	4.95	4.661	3.857	3.49	7.81	0.245	0.606	0.024	0.015

## F More details for Applications

### F.1 Preprocessing procedure of neuroscience application

We collect spike counts within a window spanning from 30 ms to 230 ms. Our analysis is confined to the experimental setting, where a certain percentage of neurons exhibit code juggling patterns when encoding dual stimuli. Our attention is specifically directed to a subset of neurons demonstrating code juggling, as identified by the Spike Count Analysis for MultiPlexing Inference (SCAMPI) model (Chen et al., 2024). The raw data consists of spike count data, which does not inherently reveal the preference for selecting between two stimuli. Therefore, we employ a Poisson mixture model to represent a neuron’s spike count, incorporating a mixing proportion  $\alpha$  to quantify the selection preference between stimuli A and B:

$$Y^{AB}|\mu^A, \mu^B \sim \int_0^1 \text{Poi}(\alpha\mu^A + (1-\alpha)\mu^B) f(\alpha) d\alpha \quad (35)$$

The model shown in equation (35) is exactly the model under Slow Juggling hypothesis in the SCAMPI model. We applied SCAMPI model and obtain an estimation of mixing density  $f(\alpha)$ , and estimation (posterior mode) of parameters  $\mu^A$  and  $\mu^B$ . Then we derive the posterior of  $\alpha$  based on Bayes’ rule, utilizing the posterior mean as an estimator of  $\alpha_i$  for each neuron at trial  $i$ . This process yields a score matrix representing the selection preference of 74 neurons across 20 trials:

$$p(\alpha|Y_i^{AB}) = \frac{\text{Poi}(Y_i^{AB}|\alpha\hat{\mu}^A + (1-\alpha)\hat{\mu}^B) f(\alpha)}{\int_0^1 \text{Poi}(Y_i^{AB}|\alpha\hat{\mu}^A + (1-\alpha)\hat{\mu}^B) f(\alpha) d\alpha} \quad (36)$$

### F.2 Extra figures from applications

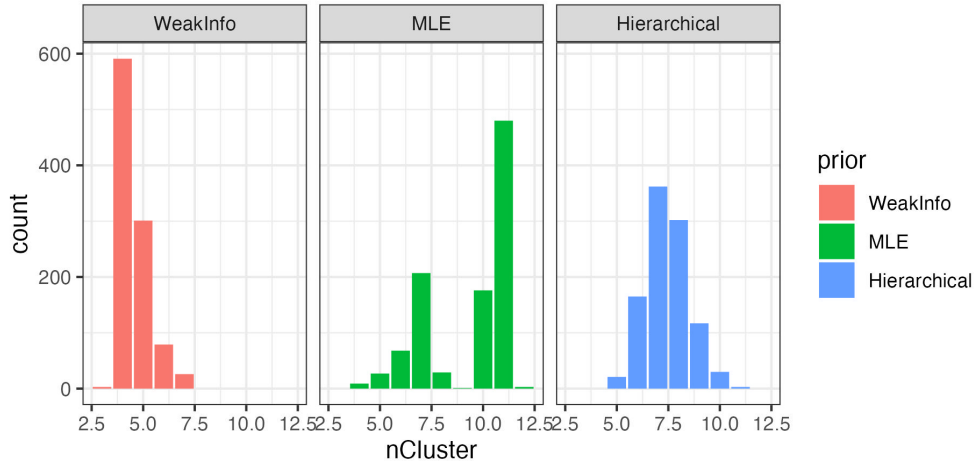


Figure 15: Posterior distributions of the number of blocks across different priors in the neural population coordination application.

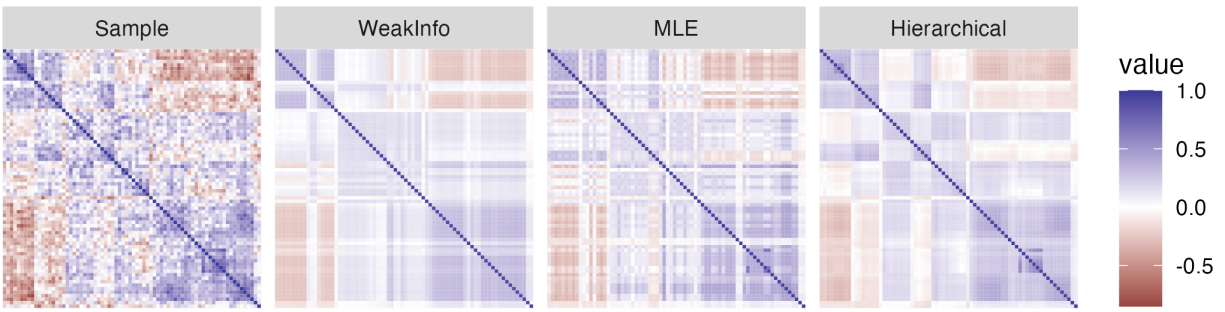


Figure 16: Covariance estimation of neural population coordination under different priors (sorted by block assignments of hierarchical prior)

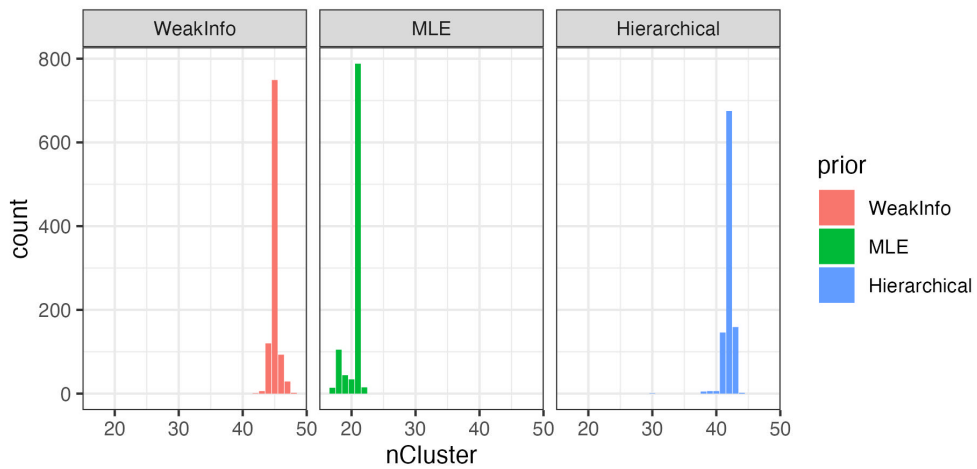


Figure 17: Posterior distribution of number of blocks under different priors in the mutual funds application.

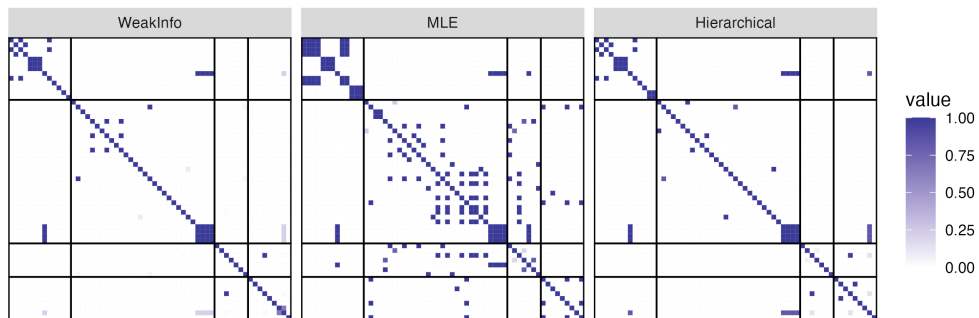


Figure 18: Posterior similarity matrix under different priors in the mutual funds application.

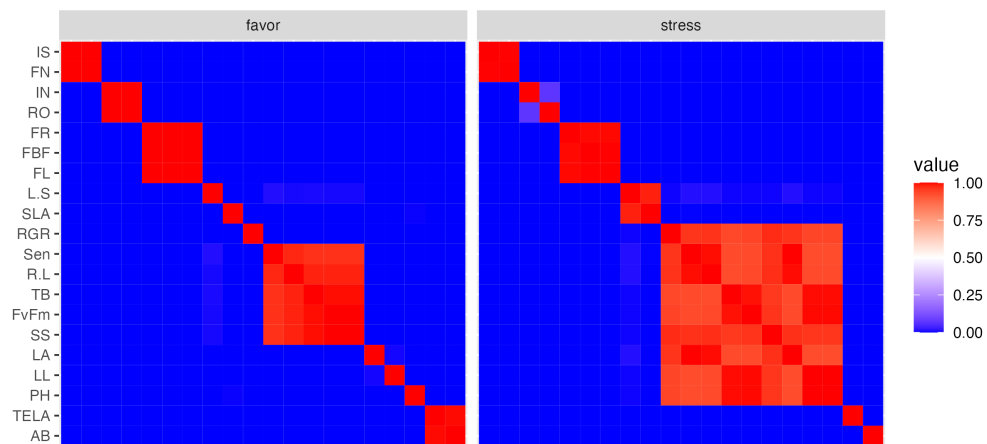


Figure 19: Posterior similarity matrices of traits under favorable and stressful environments. The number of distinct clusters decreases under drought, indicating stronger phenotypic integration.